On multilayered system dynamics and waves in anisotropic poroelastic media

Juan Pablo Parra Martinez

Doctoral Thesis

2016

MWL / Centre for ECO^2 Vehicle Design
KTH Royal Institute of Technology
Teknikringen 8
SE10044 Stockholm, Sweden

LAUM - UMR CNRS 6613
Université du Maine
Avenue Olivier Messiæn
F72085 Le Mans Cedex France

Academic thesis with permission by KTH Royal Institute of Technology, Stockholm (Sweden), and the Université du Maine, Le Mans (France), submitted for public examination for the degree of Ph.D., defended on Tuesday, December 6th 2016, at 10:00 in room F3, KTH Royal Institute of Technology, Lindstedsvägen, Stockholm (Sweden). The format of this thesis complies with the specifications listed in the International Co-tutelle agreement, ratified by the two institutions.

Thèse de doctorat avec la permission de KTH Royal Institute of Technology, Stockholm (Suède), et de l'Université du Maine, Le Mans (France), soumise pour examination publique Mardi 6 Décembre 2016, à 10h00 dans la salle F3, KTH Royal Institute of Technology, Lindstedsvägen, Stockholm (Suède) en vue de l'obtention du grade de Docteur. Le format de ce manuscript est conforme aux spécifications citées dans l'accord de Co-tutelle Internationale, signé par les deux établissements.

ISSN 1651-7660
TRITA-AVE 2016:77
ISBN 978-91-7729-172-5

Author contact: jppm@kth.se | juan.parra@univ-lemans.fr

"Goodbye," said the fox. "And now here is my secret, a very simple secret: It is only with the heart that one can see rightly; what is essential is invisible to the eye."
"What is essential is invisible to the eye," the little prince repeated, so that he would be sure to remember.
"It is the time you have wasted for your rose that makes your rose so important."
"It is the time I have wasted for my rose–" said the little prince, so that he would be sure to remember.
"Men have forgotten this truth," said the fox. "But you must not forget it. You become responsible, forever, for what you have tamed. You are responsible for your rose..."
"I am responsible for my rose," the little prince repeated, so that he would be sure to remember.

Antoine de Saint-Exupéry, *The Little Prince*.

to my nephew, Emilio.

Contents

Abstract (in english) iii
Abstract (in french). v
Abstract (in swedish) vii
Acknowledgements. ix
Preface. xi

Part 1. Overview 1

Chapter I. Introduction 3

Chapter II. Model for the wave propagation and dynamic behaviour of multilayered systems with anisotropic poroelastic layers 7
II.1 State-space representation 8
II.2 Analytical derivation of the state matrix for different media . . . 10
II.2.1 Fluid media 10
II.2.2 Anisotropic poroelastic media 11
II.3 Semi-analytical derivation of the state matrix for arbitrary linear homogeneous media 13
II.4 Solution in the eigenspace 14
II.5 Wave properties and dynamic indicators 15

Chapter III. Wave propagation in anisotropic poroelastic media 17
III.1 Waves in a human femoral bone 17
III.2 Waves in an industrial melamine foam 20

Chapter IV. Dynamics of multilayered systems with anisotropic poroelastic media 27

IV.1 Influence of the material orientation of anisotropic poroelastic cores in multilayered systems 27
IV.1.1 Dynamic behaviour 28
IV.1.2 Phenomena intrinsic to the influence of anisotropic poroelastic media in multilayered systems 31
IV.2 Optimal alignment of anisotropic poroelastic cores in a multilayered system for dynamic performances 34
IV.2.1 Multilayered system and design variables 35
IV.2.2 Optimisation problem and stability of extreme points 36
IV.2.3 Short-range frequency optimisation for acoustic performance . 37
IV.2.4 Large-range frequency optimisation for acoustic performance . 40

Chapter V. Conclusions 43

Appendix A. Matrices for the semi-analytical calculation of the state matrix in linear homogeneous media 47
A.1 Fluid (or fluid equivalent) media 47
A.2 Solid elastic media 48
A.3 Poroelastic media under the $\{\mathbf{u}^s, \mathbf{u}^t\}$ representation 49
A.4 Poroelastic media under the $\{\mathbf{u}^s, \mathbf{u}^f\}$ representation 50

Bibliography 53

Part 2. Appended publications 59

On multilayered system dynamics and waves in anisotropic poroelastic media

Abstract

This thesis proposes a method for the extended dynamic analysis of multilayered systems under arbitrary excitation, and in particular, those including anisotropic poroelastic media. This method fills a gap in the numerical methods that allow for a systematic study of both the dynamics of a multilayered system, and the phenomena intrinsic to the anisotropy of the poroelastic layers that compose it.

The approach relies on the expansion of the dynamic solution as a superposition of plane waves. The formulation is based on a state-space representation in terms of physical field variables, and directly provides the characteristics of the waves in the different layers of the structure. This method requires the computation of the state matrix of each material layer, which characterises its the dynamic state. Two methods for the derivation of the state matrix are proposed. A *term-by-term*, or analytical derivation, is presented for the acoustic analysis of fluid, solid, and poroelastic media. This approach is however unpractical and prone to errors for media where the state vector is large. Therefore, a semi-analytical derivation of the state matrix is proposed. Given its formulation, the state matrix of any type of linear homogeneous medium, including arbitrary anisotropic properties and multi-physics interactions, may be derived.

An analysis of the wave propagation in an infinite anisotropic poroelastic medium is done with respect to its orientation. A first study of the wave propagation in an anisotropic poroelastic medium where there is strong mechanical coupling between the saturating fluid and the solid frame is performed. Then, the investigation of the wave propagation in an industrial open-celled foam where the mechanical coupling between the two phases of the material is weak is done. A discussion with regards to the properties of each wave in the medium allows for the understanding of the wave phenomena induced by the anisotropy of the medium.

Through the proposed method, the influence of the anisotropy of poroelastic cores on the behaviour of the multilayered systems, as well as the dynamic phenomena within the material layers, is evaluated. The studied system is composed of an anisotropic open-celled melamine foam core in between two metal sheets. A frequency shift of the fundamental resonance of the panel is observed, and linked to the variation of the stiffness coefficient coupling compressional stresses and strains within the core with respect to its material orientation. Furthermore, the compression-shear coupling effects taking place in the poroelastic core layers are analysed. The influence of this phenomena on the overall

behaviour of the panel is correlated to the wave characteristics and amplitudes within the core. Finally, the optimisation of multilayered systems for acoustic performance in terms of sound transmission loss is presented. The systems consists in a melamine poroelastic anisotropic core within two metallic sheets. The melamine core consists on either one or two layers of equal thickness with independent material orientations. The design variables are the core material alignment angles with respect to the global coordinate system. This allows to control the phenomena related to the anisotropy of the core layers without increasing the mass of the overall system. The solution to the minimisation problem suggests the existence of a unique optimal solution in terms of material orientation regardless of the layer partitioning of the core, which may be related to the overall stiffness in compression of the core. The solution to the maximisation problem shows that the acoustic response can be improved by sectioning the core into two independently oriented poroelastic layers. The enhancement of sound transmission loss is correlated to the dynamic phenomena in the core layers in terms of relative deformation. An alternative optimisation problem may defined in terms of shear-compression coupling. Its solution differs in terms of overall acoustic performance of the panel, but may be exploited for the tuning of the acoustic behaviour at particular frequencies.

Keywords: poroelastic media, anisotropy, plane waves, multilayered systems, dynamics, acoustics, optimisation.

Dynamique de systèmes multicouches et ondes dans des milieux poro-élastiques anisotropes

Résumé

L'anisotropie des propriétés mécaniques et acoustiques des matériaux poro-élastiques est un facteur déterminant dans le comportement de panneaux utilisés dans différents domaines de l'ingénierie. La compréhension des différents mécanismes physiques conditionnant la réponse en fréquence de ces structures est alors nécessaire. L'anisotropie intrinsèque des matériaux poreux visco-élastiques présente un potentiel particulier pour l'optimisation multi-fonctionnelle de parois multicouches. En effet, ces parois doivent souvent respecter des contraintes de raideur et isolation sonore et thermique de manière simultanée. Une méthode par superposition d'ondes planes dans des parois composées de matériaux poro-visco-élastiques est présentée afin d'analyser la sensibilité de la réponse acoustique de structures multicouches à l'alignement relative des couches poreuses anisotropes dans celles-ci. La méthode est validée et appliquée à l'étude d'un système composée d'une mousse de mélamine située entre deux parois métalliques. Ce système permet d'illustrer des phénomènes intrinsèques aux couche poro-élastiques anisotropes, tel que le décalage en fréquence de la résonance fondamentale du système, et les couplages de compression-cisaillement dans le milieu poro-élastique. Ce phénomène de couplage est particulièrement intéressant puisqu'il n'est caractérisable que par la polarisation des ondes dans le milieu poro-élastique anisotrope. En fin, la méthode est appliquée afin d'optimiser un système multicouche pour des performances acoustiques. Les variables d'optimisation sont les orientations relatives des couches poro-élastiques anisotropes par rapport au système de coordonnées globales. Les solutions aux problèmes d'optimisation sont analysées en termes de comportement mécanique, ce qui permet d'établir une corrélation entre performances acoustiques et comportement dynamique.

Mots-clés: matériaux poro-visco-élastique, anisotropie, ondes planes, panneaux multicouches, dynamique, acoustique, optimisation.

On multilayered system dynamics and waves in anisotropic poroelastic media

Sammanfattning

Den mekaniska och akustiska anisotropin är styrande för hur materialegenskaperna i ett flerskikt-system beter sig. Förståelsen av de mekanismer som styr ett flerskiktssystems dynamiska egenskaper är av största vikt. För poroelastiska material möjliggör dess inneboende anisotropi en optimering av multifunktionella system. Sådana system är begränsade av dess prestanda vad gäller styvhet, termisk koppling och akustiska egenskaper. En planvågsmetod presenteras för att studera riktningsberoendet för de dynamiska egenskaperna i anisotropa poroelastiska material, när de används i flerskiktssystem. Metoden tillämpas på ett system med en anisotrop kärna av melaminskum med öppna celler placerad mellan två metallskikt. Denna konfiguration möjliggör studier av de fenomen som uppstår då anisotropa poroelastiska material används i flerskiktssystem, exempelvis förflyttning av panelens grundresonansfrekvens och kopplingseffekter mellan kompression och skjuvning i den poroelastiska kärnan. Det senare fenomenet är speciellt viktigt eftersom grundar sig i en okonventionell polarisering av vågor i anisotropa poroelastiska material. Metoden är slutligen anpassad för en optimering av de akustiska egenskaperna i flerskiktssystem. Variablerna för denna optimering är således kärnmaterialets riktning relativt ett globalt koordinatsystem. Optimeringsproblemets lösningar analyseras med avseende på dynamiska egenskaper vilket gör det möjligt att korrelera de akustiska egenskaperna för det övergripande systemet till responsen för vardera skikt separat.

Nyckelord: Poroelastiska material, anisotropi, planvågor, flerskiktssystem, dynamik, akustik, optimering

Acknowledgements

I started the project in September 2012 with the conviction that anyone could do a doctoral thesis. Even though I could only be in awe those who had achieved it, I was sure that, if you gave comfortable funding to someone with a structured academic background, the success of a doctoral thesis would be a matter of commitment and a fair share of caffeine.

I have never stood so corrected.

I have had to humbly realise how little I know, to learn how to take the (far too many) punches of frustration -if the code doesn't work, it is not the code's fault, nor the computer's, nor the table's, nor ...- and that no one can do this alone. I was right about the caffeine though.

After four and a half years of travelling between Stockholm and Le Mans -with the odd trip to Brussels, Göteborg and Toulouse- and constantly challenging my brain and my psyche, the achievement of this manuscript represents, by far, the biggest challenge I have ever faced, and many people helped me to get through it.

I am deeply thankful to those who became my mentors and friends: Peter, Olivier and Jacques. Thank you for the chance you gave me, for your trust, your interest, and, most of all, for the patience you have shown whilst dealing with someone as stubborn as me. You have taught me what the rollercoaster of research is, and to enjoy the ride. *Tack. Merci. Gracias.*

I am also very thankful to Ulrika Ohlsson (Volvo Trucks), for the warm and friendly welcome to Göteborg and to Volvo Trucks, and Per Wennhage, for the long talks and inspiring my curiosity in a large matter of subjects. This thesis would not have been possible without your valuable input.

I am thankful to KTH and U. Maine for their support, specially the people in the MWL Laboratory, the LAUM, and the Centre for ECO^2 Vehicle Design. The latter is acknowledged for the funding of the project.

During the thesis work, I have had the chance to receive also funding from the Petersohn Memorial Foundation at KTH, the Collège Doctoral from the U. Maine, and the Institut Français de Suède in Stockholm, to whom I am very grateful.

For the times spent in Stockholm, I thank the amazing people who are, or who have been part of the life in at Teknikringen 8. You have made my life in the lab, and in Stockholm, pretty incredible. I have to thank specially Rickard, Malin, and Anna, for making me feel like home, something I was longing since leaving Toulouse; and Luck Peerlings for all the fun times in and out of the office. Also, thank you Andrew Marais for making any effort of getting fit completely useless.

For the time spent in Le Mans, I have to thank Olivier and Claire for all their support, as well as all the people in the LAUM. I thank Julien, Margaux and Côme, for all the beers, *rillettes*, burgers, and awesome times since 2011. Also, I kindly thank the Latrouite family (Antoine, Camille, Constance, Agathe, Estelle and Laurent) for the warm welcome to their house and friendship. *Je resterai à jamais le petit Colombien au fond du jardin. Merci!*

Finally, this thesis would not have been possible without the unconditional support from my family, specially from Juanita and Isabel, and my closest friends, Cyril, Jean, Alex and Michel. Thank you for not letting me get lost in the labyrinths of my work and my head, for being my anchor to reality, and reminding me what really matters.

Juan Pablo Parra Martinez,
Stockholm, 2016.

Preface

The work presented in this thesis was funded by the *Centre for ECO*^{2} *Vehicle Design* and carried out as part of the international agreement of co-tutelle between the **KTH Royal Institute of Technology** (Stockholm, Sweden), and the **Université du Maine** (Le Mans, France).

The main supervision of this work was performed by Prof. Peter Göransson, Ph.D.[(i)] and Prof. Olivier Dazel, Ph.D.[(ii)]. The co-supervision was performed by Jacques Cuenca, Ph.D. [(iii)] and Assoc.-Prof. Per Wennhage, Ph.D.[(iv)]

The examination committee is composed of Assoc.-Prof. Camille Perrot, Ph.D-H.D.R. (opponent, *rapporteur*)[(v)], Prof. Philippe Leclaire, Ph.D.[(vi)] (jury, *rapporteur*), Prof. Maria Heckl, Ph.D.[(vii)] (jury), and Prof. Ulf Olofsson, Ph.D.[(viii)] (jury).

The thesis consists in two parts. The first part gives an overview of the research with a summary of the work performed. The second part collects the following scientific publications:

[**I**] Parra Martinez, J. P., Dazel, O., Göransson, P., & Cuenca, J. (2016). **Acoustic analysis of anisotropic poroelastic multilayered systems**, Journal of Applied Physics, 119(8), 084907;

[**II**] Parra Martinez, J. P., Dazel, O., Göransson, P., & Cuenca, J. (2016). **Derivation of the state matrix for dynamic analysis of linear homogeneous media**, Journal of the Acoustical Society of America - Express Letters, 140(2),

[(i)]Department of Aeronautical and Vehicle Engineering, KTH Royal Institute of Technology, Teknikringen 8, SE-10044 Stockholm, Sweden, *pege@kth.se*

[(ii)]LAUM Laboratoire d'Acoustique de l'Université du Maine - UMR CNRS 6613, Avenue Olivier Messiaen, F-72085 Le Mans Cedex France, *olivier.dazel@univ-lemans.fr*

[(iii)]Siemens Industry Software, Interleuvenlaan 68, B-3001 Leuven, Belgium, and Department of Aeronautical and Vehicle Engineering, KTH Royal Institute of Technology, Teknikringen 8, SE-10044 Stockholm, Sweden, *jcuenca@kth.se - jacques.cuenca@siemens.com*

[(iv)]Department of Lightweight Structures, KTH Royal Institute of Technology, Teknikringen 8, SE-10044 Stockholm, Sweden, *wennhage@kth.se*

[(v)]Laboratoire de Modélisation et Simulation Multi Echelle UMR 8208 CNRS Université Paris-Est Marne-la-Vallée Cedex 2, France, *Camille.Perrot@univ-paris-est.fr*

[(vi)]DRIVE EA1859, Univ. Bourgogne Franche Comté, F58000 Nevers, France, *Philippe.Leclaire@u-bourgogne.fr*

[(vii)]School of Computing and Mathematics, Keele University, Staffordshire, ST5 5BG, United Kingdom, *m.a.heckl@keele.ac.uk*

[(viii)]Department of Machine Design, KTH Royal Institute of Technology, Brinellvägen 83, SE-10044 Stockholm, Sweden, *ulf.olofsson@itm.kth.se*

p. EL218-EL220;

[**III**] Parra Martinez, J. P., Göransson, P., Dazel, O., Cuenca, J. & Jaouen, L. (2016). **Wave analysis of intrinsic phenomena related to anisotropic poroelastic materials in multilayered systems**, in Proceedings of ISMA 2016 International Conference in Noise and Vibration Engineering and USD 2016 International Conference on Uncertainty in Structural Dynamics, Leuven, Belgium, Sept. 19-21, 2016;

[**IV**] Parra Martinez, J. P., Cuenca, J., Göransson, P. & Dazel, O. (2016). **Optimal alignment of anisotropic poroelastic cores in multilayered systems for acoustic performance**, to be submitted.

Parra Martinez performed the analytical and numerical work for all the publications, under the scientific methodology agreed upon with the co-authors. The numerical implementation of the diffuse field model was performed in collaboration with Jaouen. The methods and results were discussed and analysed by all authors, from where the first drafts of the publications were based upon. Parra Martinez then produced the publications under iterative interaction with all the co-authors. Additionally, the third publication was presented by the author in the conference therein stated.

The following works were produced as part of the doctoral project, but are not included in this thesis:

[**V**] Parra Martinez, J.P., Dazel O., Göransson, P., & Cuenca, J. **Analyse d'ondes, puissances internes et performance acoustique de matériaux poroélastiques dans des panneaux multicouches**, in Proceedings of Congrès Français d' Acoustique 2016, Le Mans, France, Apr. 11-15, 2016;

[**VI**] Parra Martinez, J.P., Dazel, O., Göransson, P. & Cuenca, J. **Calculation of internal powers for anisotropic porous materials within multilayered structures based on plane wave approximation**, in Proceedings of Euronoise 2015, Ed., Maastricht, Netherlands, June 1-3, 2015;

[**VII**] Parra Martinez, J.P., Dazel O., Göransson, P., & Cuenca, J. **Modélisation de panneaux multicouches composés de matériaux poro-élastiques anisotropes par méthodes d'ondes planes**, in Proceedings of Congrès Français de Mécanique 2015, Lyon, France, Aug. 24-28, 2015;

[**VIII**] Parra Martinez, J.P., Göransson, P., Dazel, O. & Cuenca, J. **Acoustic Response modelling of Multilayered Structures with Anisotropic Porous materials**, in Proceedings of SAPEM 2014 Symposium On The Acoustics Of Poro-Elastic Materials, Stockholm, Sweden, Dec. 16-18, 2014;

[**IX**] Parra Martinez, J.P., Göransson, P., Dazel, O. & Cuenca, J. **Analysis of the frequency response behaviour of anisotropic multilayered structures and potential acoustic performance optimizations**, in Proceedings of ISMA 2014 International Conference in Noise and Vibration Engineering and USD 2014 International Conference on Uncertainty in Structural Dynamics, Leuven, Belgium, Sept. 15-17, 20144375-4386.

All conference proceedings were presented by Parra Martinez in the venues therein stated.

As part of the PhD project, the degree of Licentiate in Technology was awarded in 2015 by KTH Royal Institute of Technology to the author for the thesis **On the ECO^2 multifunctional design paradigm and tools for acoustic tailoring**[42].

Part 1

Overview

Chapter I

Introduction

The instability of petrol prices and the increasing concerns related to global warming have forced aeronautical and vehicle industries to invest in research in favour of environmentally-friendly and economical production processes and methods. Moreover, the legislative pressure on vehicle manufacturers has been important in the past decade. For example, the failure to respect toxic particle emissions limitations on new vehicle designs[(i)] carries severe economical penalties for the car manufacturers[(ii)].

In order to fulfil legal requirements and remain competitive, aeronautical and vehicle manufacturers have introduced novel solutions ranging from the re-dimensioning of transport infrastructures for optimised haulage[(iii)], to the use of lightweight materials [23,65], all supported by an increasing usage of computational tools [29].

The conventional design paradigm relies on sequential evaluations of systems with respect to individual performances. Following a Ford-type method (*i.e.* sequential chain of production), the design partially depends on the negotiation skills of the designers. As a consequence, the vehicle assembly consists of a load carrying body-in-white to which several layers of materials and structures are added, each layer fulfilling an individual requirement. This conventional paradigm, even though efficient with regard to particular performances, is prone to being costly regarding weight, consequently increasing the fuel consumption and decreasing the haulage capacity of the vehicle.

[(i)] *Reducing CO2 emissions from passenger cars*. European Commission (Climate Action). `http://ec.europa.eu/clima/policies/transport/vehicles/cars/index_en.htm`

[(ii)] In September 2015, the United States Environmental Protection Agency publicly notified Volkswagen Group of their violation of a federal law (ClearAir Act) with regards to intentionally manipulating a polluting-emissions software. The settlement cost the company 14.7 billion USD. Other worldwide legal and financial repercussions are expected.

[(iii)] Scania Group, in collaboration with Siemens, opened in June 2016 the first road with overhead power lines in Gävle (Sweden), and has equipped several trucks with pantograph collectors which allow the trucks to function under electric power, considerably reducing the environmental and economical footprint of their operational regime.

To fulfil a larger range of functionalities without penalising the fuel or transport efficiency of the vehicle, a shift to a design paradigm based on the optimisation for multi-functional performance is currently explored. This method relies on the iterative evaluation of several functions (cost, fatigue, dynamic behaviour, etc.), adapting (choosing or designing) the materials and structures until the completed vehicle concept fulfils the set requirements. [10,66]. The aerospace industry, for example, has replaced materials like steel, titanium and aluminium, to topologically-optimised lightweight hybrid materials [55], such as fibre-composite materials, or honeycomb structures [39].

Moreover, novel material modelling and characterisation techniques [17,47,62] open the possibility to include complex phenomena in the design paradigm, such as the influence of temperature gradients or flow on the behaviour of poroelastic materials [24], amongst others [35,41,52]. This has enabled the study of more realistic structures. An example of numerical methods commonly used is the Finite-Element Method [30,33] which is versatile although costly in terms of computational efforts. Consequently, there is a need for computationally efficient methods that reflect the phenomena intrinsic in complex yet real material models.

Additionally, most porous materials used in aeronautical and vehicle engineering applications exhibit a certain degree of anisotropy inherent to manufacturing processes. The modelling of the behaviour of such materials is such that isotropic approximations fail to provide sufficient insight into the different phenomena involved [2,13,31,51]. For critical functions this could result in unacceptable designs, and studies on multilayered finite-sized systems clearly demonstrate that anisotropy can significantly alter the dynamic behaviour of a poroelastic material [34]. Thus, there is a need for tools to correlate the dynamic behaviour of the multilayered system with critical performance in terms of dissipative and kinetic phenomena within the anisotropic material layers.

To contribute to meeting the needs for numerical methods to study the dynamics of multilayered systems and the phenomena intrinsic to anisotropic poroelastic material layers, this thesis focuses on three objectives. The first objective is to develop a model for the dynamic behaviour of multilayered systems including anisotropic poroelastic media. Using this method, the second objective is to study the physical phenomena taking place in the different layers composing such structures. The last objective is to study the optimisation of multilayered systems with anisotropic poroelastic cores for acoustic performance.

The manuscript is organised as follows.

Chapter II presents the mathematical background, which relies on a state-space representation. Two different methods to derive the state matrix of a medium are proposed. The first method is focused on a *term-by-term*, or analytical derivation, for the

acoustic analysis of fluid, solid, and poroelastic media. The second method is corresponds to a semi-analytical derivation, which is an extension of the state-space representation for the dynamic analysis of any type of linear homogeneous medium, including arbitrary anisotropic properties and multi-physics interactions.

Chapter III presents a detailed study of the wave propagation in anisotropic poroelastic media. First, a validation of the semi-analytical derivation of the state matrix is presented. The calculation of wave properties in an infinite poroelastic medium with strong fluid/solid dynamic coupling is validated against a wave propagation model available in the literature. Thereafter, the wave propagation problem is solved in the case of an anisotropic industrial melamine foam, and the nature of the waves propagating in such media is discussed.

Chapter IV studies the dynamic behaviour of several multilayered configurations using the proposed model. First, the dynamic analysis of a multilayered system with a core composed of the melamine foam previously studied is performed. The proposed method is used to access the physical field variables, as well as the properties and contributions of the waves in each layer. A particular interest is given to the influence of the anisotropic material core orientation on the dynamic behaviour of the panel. This allows the investigation of phenomena inherent to anisotropic poroelastic media, like compression-shear motion coupling, and the shift in the fundamental resonance frequency of the panel. Finally, a study of the optimal material alignment of anisotropic poroelastic cores of a multilayered system for dynamic performance is presented. The performance of the panel is measured in terms of sound transmission loss within a range of frequencies. The solutions to the optimisation problem are analysed in terms of dynamic response of the cores, and the stability of the solution in terms of small variations of the design variables, probing the governing physical phenomena behind the optimal configurations. In this way, the Pareto optimal solution is determined as a compromise between the value of cost function at the solution and its robustness. The phenomena governing the response of system and the Pareto optimal solution are used to construct an alternative optimisation problem, where the performance is measured by the dynamic response of the anisotropic poroelastic cores.

Conclusions are given in Chapter V, where also a perspective of further applications and future work is presented.

Chapter II

Model for the wave propagation and dynamic behaviour of multilayered systems with anisotropic poroelastic layers

The multilayered systems used for aeronautical and vehicle engineering applications are usually composed of several layers, fulfilling a large range of functionalities. From a mechanical perspective, one of the roles fulfilled by such panels is the control of sound absorption and transmission. Most common sound-absorbing poroelastic materials are composed of a porous solid skeleton saturated by air. This enables energy dissipation through different mechanisms such as viscous effects, thermal effects and structural damping. The dynamic behaviour of a fluid-saturated poroelastic medium can be described under the modelling paradigm established by Biot[7–9]. This theory, originally developed for geophysical applications, has been shown to be successful for characterising and predicting the behaviour of isotropic sound-absorbing materials in a wide range of problems[27,49].

Regarding acoustic and mechanical behaviour of anisotropic poroelastic media, fundamental publications by Biot[4–6], and more recent works by Melon *et al.*[36,37], or Allard *et al.*[1], amongst others[14,26,48,59], set the basis for the current models.

The study of multilayered panels including anisotropic porous materials requires a combination of physical models and simulation techniques. As discussed in the introduction, a commonly used method is the Finite Element Method[30], specially in the low frequency regime. Semi-analytical formulations have been developed for the mechanical behaviour of seismic waves in unbounded media[11,54]. However, the physical phenomena induced by coupling finite-sized anisotropic porous media to other media in bounded panels has not been addressed. Furthermore, Khurana *et al.*[32] extended the Transfer Matrix Method (TMM) to transverse isotropic porous materials in multilayered structures. This particular case of anisotropy allows for an analytical solution of the

dispersion relation governing the wavenumbers of the waves travelling in the medium. Another example is the recent paper by Allard *et al.*[3], where the authors extended the method of Khurana *et al.* to transverse isotropic porous media whose plane of symmetry differs from the plane of incidence. Thus, the wave amplitudes were analytically evaluated in the layer by referring to a similar geometry to that in Khurana's work. As in previous geophysical studies, neither the transfer matrix nor the acoustic behaviour of bounded orthotropic porous media were addressed, and the extension of such methodologies to fully anisotropic media would yield cumbersome and thus impractical expressions. This highlights the fact that a numerical approach is inevitable at least in some stages of the method in order to assess a complete, accurate and reliable picture of wave propagation in bounded fully anisotropic poroelastic media.

Having access to computational tools, the understanding of the mechanical and dissipative phenomena linked to the behaviour of anisotropic multilayered structures may be enhanced. Based on works by Biot[4–6], Carcione[11] developed an advanced model for the free field propagation of elastic waves through anisotropic porous media for geophysical purposes, allowing for the calculation of energy quantities in such media. There is however a gap in the tools for the systematic computation of the dynamic behaviour of panels, as well as the energy balance and wave properties in bounded material layers.

This chapter presents a model for the dynamic behaviour of multilayered structures with linear homogeneous media, in particular anisotropic poroelastic media, in terms of physical field variables and wave field characteristics.

In the following, the scalar quantities are denoted in normal font, and the tensors are denoted in bold font. When convenient, a definition of the dimensions for tensors is expressed under the form $[\in \mathbb{C}^{u\times v}]$, where u and v are the dimensions. The convention $\imath = \sqrt{-1}$ is used in the manuscript. Note that, for consistency purposes, the nomenclature of some terms in this thesis differs to that of the appended publications.

II.1 State-space representation

The dynamic state of a linear homogeneous medium, under harmonic excitation of circular frequency ω, may be described in general by a system of m partial derivative equations with respect to space on the physical field variables chosen to represent the medium in a Cartesian coordinate system xyz,

$$\left[\mathbf{A}_0 + \mathbf{A}_x \frac{\partial}{\partial x} + \mathbf{A}_y \frac{\partial}{\partial y} + \mathbf{A}_z \frac{\partial}{\partial z}\right] \mathbf{w}(x, y, z) = \mathbf{0}, \tag{1}$$

where $\mathbf{w}(x, y, z) \in \mathbb{C}^m$ is the vector composed of physical fields necessary to model the medium; and the matrices $\{\mathbf{A}_i \in \mathbb{C}^{m\times m}\,,\ i = \{0, x, y, z\}\}$ are known, and depend on the frequency.

An excitation of the system by a plane wave prescribing the wavenumbers k_x and k_y is considered. Therefore, an arbitrary physical field $v \in \mathbf{w}$, can be written as

$$v(x, y, z, t) = v(z)\, \mathrm{e}^{\imath\left(\omega t - k_x x - k_y y\right)}. \tag{2}$$

As a consequence of the harmonic plane wave excitation, the system in Eq. (1) may be rewritten as

$$\left[\mathbf{R} + \mathbf{A}_z \frac{\partial}{\partial z}\right] \mathbf{w}(z)\, \mathrm{e}^{\imath\left(\omega t - k_x x - k_y y\right)} = \mathbf{0}, \tag{3}$$

where $\mathbf{R} = \mathbf{A}_0 - \imath k_x \mathbf{A}_x - \imath k_y \mathbf{A}_y$. Let n be the rank of the system, with $n \leq m$. The analytical expressions of the matrices $\{\mathbf{A}_i\,,\ i = \{0, x, y, z\}\}$ can be found in Appendix A for the dynamic modelling of fluid, anisotropic solid, and anisotropic poroelastic media.

As the term $\mathrm{e}^{\imath\left(\omega t - k_x x - k_y y\right)}$ is common to all physical fields, it will be omitted in the following in order to simplify the notation.

The vector $\mathbf{w}(z)$ has $n \leq m$ linearly independent variables. The solution of the system corresponds to finding an expression for the partial derivative over z of $\mathbf{w}(z)$. A direct solution of Eq. (3) is not possible as the matrix $\mathbf{A}_z$ is singular. $\mathbf{w}(z)$ is partitioned in such a way that the n linearly independent physical fields compose a vector $\mathbf{s}(z) \in \mathbb{C}^n$, often called state vector. Let $\mathbf{s}_0(z) \in \mathbb{C}^q$, where $q = m - n$, be the vector composed of the remaining field variables.

It is important to note that, for a particular medium, the choice of the variables in the state vector $\mathbf{s}(z)$ is not unique: the field variables depend on the equations governing the media. Only the length of the state vector is unique to the physics of the problem, and is equal to the rank of the system of equations governing the state of the medium.

An example of such vector partitioning may be illustrated by analysing the three equations of motion and the constitutive law governing the dynamic state of a perfect fluid,

$$-\nabla p = -\omega^2\, \rho_f\, \mathbf{u}^f, \tag{4}$$

$$p = -K_f\, \nabla \cdot \mathbf{u}^f, \tag{5}$$

where ρ_f and K_f are the fluid density and compressibility, p is the pressure, and $\mathbf{u}^f \in \mathbb{C}^3$ is the vector of fluid particle displacements.

Under the plane wave expansion assumption as described in Eq. (2), the rank of the system of Eqs. (4) and (5) is equal to 2. Therefore, the state vector $\mathbf{s}(z)$ will be of length equal to 2. Moreover, if the system of equations is written in terms, for example, of pressure and particle velocities, the state vector would include exclusively the pressure

and the particle velocity on the $z-$axis, as these are the physical field variables with which boundary conditions are written. Consequently, the vector $\mathbf{w}(z)$ may be partitioned into

$$\mathbf{w}(z) = \{\mathbf{s}_0(z) \mid \mathbf{s}(z)\}^{\mathrm{T}} = \left\{u_x^f(z)\ u_y^f(z) \mid u_z^f(z)\ p(z)\right\}^{\mathrm{T}}. \tag{6}$$

The state of the medium is then uniquely defined by the evolution with respect to z of the the state vector $\mathbf{s}(z)$, which enables the rewriting of the problem in the form of the state-space representation [19,53,64], where the evolution of the fields can be described solely as a function of the state vector:

$$\frac{\partial}{\partial z}\mathbf{s}(z) = -\boldsymbol{\alpha}\,\mathbf{s}(z), \tag{7}$$

where $\boldsymbol{\alpha} \in \mathbb{C}^{n\times n}$ is called the state matrix, and depends only on the material parameters, frequency, and prescribed wavenumbers k_x and k_y. The latter representation allows for the modelling of the dynamic state of a system, as a direct solution of Eq. (7) yields the transfer matrix $\mathbf{M}(z, z_0)$ between two points of coordinates z_0 and z,

$$\mathbf{M}(z, z_0) = \mathbf{e}^{-(z-z_0)\boldsymbol{\alpha}}, \tag{8}$$

where $\mathbf{e}^{[.]}$ is the exponential matrix operator. To proceed, the derivation of the state matrix $\boldsymbol{\alpha}$ is required. Therefore, linear relations between the variables in $\mathbf{s}_0(z)$ and $\mathbf{s}(z)$ need to be established from Eq. (3) in order to calculate the partial derivatives of the fields in the state vector.

II.2 Analytical derivation of the state matrix for different media

A straightforward method to derive the state matrix is a *term-by-term*, or analytical, derivation, for each material model studied.

II.2.1 Fluid media

The equations governing the dynamic state of a perfect fluid medium, see Eqs. (4) and (5), may be used to define the state vector, see. Eq. (6). The state matrix $\boldsymbol{\alpha} \in \mathbb{C}^{2\times2}$ for a perfect fluid medium relates $\partial u_z^f(z)/\partial z$ and $\partial p(z)/\partial z$ as a function of $u_z^f(z)$ and $p(z)$.

From the projection of Eq. (4) on z, the partial derivative over z of the pressure may be expressed as

$$\frac{\partial p(z)}{\partial z} = \omega^2\,\rho_f\,u_z^f(z). \tag{9}$$

The term $\dfrac{\partial u_z^f(z)}{\partial z}$ may be derived from the constitutive law in Eq. (5)

$$\frac{\partial u_z^f(z)}{\partial z} = -\frac{p(z)}{K_f} + \imath k_x u_x^f(z) + \imath k_y u_y^f(z). \tag{10}$$

The terms $u_x^f(z)$ and $u_y^f(z)$ may be then expressed as a function of the field variables in $\mathbf{s}(z)$, which can be done from the projection of Eq. (4) in x and y,

$$u_x^f(z) = -\frac{\imath k_x}{\omega^2 \rho_f} p(z), \tag{11}$$

$$u_y^f(z) = -\frac{\imath k_y}{\omega^2 \rho_f} p(z). \tag{12}$$

Thus, the state matrix for a perfect fluid medium is

$$\boldsymbol{\alpha} = \begin{bmatrix} 0 & -\dfrac{1}{K_f} + \dfrac{k_x^2 + k_y^2}{\omega^2 \rho_f} \\ \omega^2 \rho_f & 0 \end{bmatrix}. \tag{13}$$

II.2.2 Anisotropic poroelastic media

In a similar way, the state matrix for a poroelastic, or solid, medium may be derived. The analytical expression of the state matrix for an isotropic media has been presented in the literature[19]. There, the terms dependent on k_y are neglected as the material behaviour is independent of the azimuthal angle of incidence of the excitation.

In general, poroelastic media may be modelled via the paradigm established by Biot[7,8]. Several representations that model the coupling between the solid skeleton and the saturating fluid exist in the literature. Here, the $\{\mathbf{u}^s, \mathbf{u}^t\}$ representation[18] is adopted, but the procedure for the derivation of the state matrix for the $\left\{\mathbf{u}^s, \mathbf{u}^f\right\}$ representation, or other, is essentially the same.

The equations governing the dynamic state of an anisotropic poroelastic medium are

$$\nabla \cdot \hat{\boldsymbol{\sigma}}^s = -\omega^2 \tilde{\boldsymbol{\rho}}_s \mathbf{u}^s - \omega^2 \tilde{\boldsymbol{\rho}}_{eq} \tilde{\boldsymbol{\gamma}} \mathbf{u}^t, \tag{14}$$

$$-\nabla p = -\omega^2 \tilde{\boldsymbol{\rho}}_{eq} \tilde{\boldsymbol{\gamma}} \mathbf{u}^s - \omega^2 \tilde{\boldsymbol{\rho}}_{eq} \mathbf{u}^t, \tag{15}$$

$$\hat{\boldsymbol{\sigma}}^s = \mathbf{H}\, \boldsymbol{\epsilon}^s, \tag{16}$$

$$p = -\tilde{K}_{eq} \nabla \cdot \mathbf{u}^t, \tag{17}$$

where $\mathbf{u}^s$, $\mathbf{u}^f$ and $\mathbf{u}^t$ are respectively the displacement fields of the solid and fluid phases, and the total displacement fields, and are related by the porosity of the foam

ϕ as $\mathbf{u}^t = \phi\,\mathbf{u}^f + (1-\phi)\,\mathbf{u}^s$; $\boldsymbol{\epsilon}^s$ and $\boldsymbol{\sigma}^s$ are the porous solid Cauchy strain and stress vectors; and p is the pore pressure. The scalar quantity $\tilde{K}_{eq}$ is the compressibility of the equivalent fluid model, modified to take into account the thermal dissipative phenomena through thermal effects.

The poroelastic media considered are fully anisotropic, thus the complex terms $\tilde{\boldsymbol{\rho}}^s$, $\tilde{\boldsymbol{\rho}}^{eq}$ and $\tilde{\boldsymbol{\gamma}}$ are second order symmetrical tensors. $\mathbf{H}$ is the Hooke's tensor of the solid phase of the material. The anisotropy is also reflected in the flow resistivity $\boldsymbol{\sigma}^{\text{flow}}$, which is a second order symmetrical tensor, from which are derived several porous parameters (see Refs. [1,18,30,32] for isotropic media, which have been extended to anisotropic media [30]).

From the equations governing the behaviour of the medium, and the assumed plane wave expansion of the form of Eq. (2), the vector of physical field variables $\mathbf{w}(z)$ may be divided into

$$\mathbf{s}_0(z) = \left\{u_x^t(z)\ u_y^t(z)\ \hat{\sigma}_{xx}(z)\ \hat{\sigma}_{yy}(z)\ \hat{\sigma}_{xy}(z)\right\}^{\mathrm{T}}, \tag{18}$$

$$\mathbf{s}(z) = \left\{u_x^s(z)\ u_y^s(z)\ u_z^s(z)\ u_z^t(z)\ \hat{\sigma}_{zz}(z)\ \hat{\sigma}_{yz}(z)\ \hat{\sigma}_{xz}(z)\ p(z)\right\}^{\mathrm{T}}. \tag{19}$$

From the latter, it is clear that the analytical derivation of the relations expressing the partial derivative over z of the state vector physical fields, as was done in Eqs. (11) and (12), could be quite cumbersome. In general, for material models when the length of the state vector becomes large, the analytical derivation of $\boldsymbol{\alpha}$ is prone to errors. Moreover, when the studied system includes physical phenomena of different nature, the number of governing coupled equations may be large, rendering the isolation of the state vector difficult. The analytical derivation of the state matrix becomes impractical, and sometimes even impossible.

An alternative approach is to manipulate the different terms in the equations of motion and constitutive laws in matrix form. The details of the analytical derivation of the state matrix for anisotropic poroelastic media may be found in Parra Martinez *et al.* [43]. The expression of the state matrix $\boldsymbol{\alpha}$ is quite involved, and is only valid for the case of the dynamic modelling of poroelastic media under the $\{\mathbf{u}^s, \mathbf{u}^t\}$ representation. An generalisation of a method that relies in an *term-by-term* derivation is not evident.

Therefore, the use of a semi-analytical derivation method, as presented in the following section, is advised.

II.3 Semi-analytical derivation of the state matrix for arbitrary linear homogeneous media

The generalised un-symmetric eigenvalue problem associated to $\mathbf{R}$ and $\mathbf{A}_z$ in Eq. (3) can be written as

$$\mathbf{A}_z = \mathbf{R}\boldsymbol{\Phi}\boldsymbol{\Lambda}\boldsymbol{\Gamma}, \qquad \boldsymbol{\Gamma} = \boldsymbol{\Phi}^{-1}, \tag{20}$$

where $\boldsymbol{\Lambda} \in \mathbb{C}^{m\times m}$ is the diagonal matrix of m eigenvalues, and $\boldsymbol{\Phi} \in \mathbb{C}^{m\times m}$ is a matrix of eigenvectors, corresponding to Eq. (20). Due to the rank deficiency, $q = m - n$ eigenvalues in $\boldsymbol{\Lambda}$ are equal to zero. Thus, reordering the eigenvectors such that the first n columns in $\boldsymbol{\Phi}$ and the first n rows in $\boldsymbol{\Gamma}$ correspond to the non-zero eigenvalues yields,

$$\boldsymbol{\Lambda} = \begin{bmatrix} \boldsymbol{\Lambda}_n & \mathbf{0}_{nq} \\ \mathbf{0}_{qn} & \mathbf{0}_{qq} \end{bmatrix}, \qquad \boldsymbol{\Phi} = [\boldsymbol{\Phi}_n \;\; \boldsymbol{\Phi}_0], \qquad \boldsymbol{\Gamma} = \begin{bmatrix} \boldsymbol{\Gamma}_n \\ \boldsymbol{\Gamma}_0 \end{bmatrix}, \tag{21}$$

where $\boldsymbol{\Lambda}_n \in \mathbb{C}^{n\times n}$, $\boldsymbol{\Phi}_n \in \mathbb{C}^{m\times n}$, $\boldsymbol{\Gamma}_n \in \mathbb{C}^{n\times m}$, $\boldsymbol{\Phi}_0 \in \mathbb{C}^{m\times q}$ and $\boldsymbol{\Gamma}_0 \in \mathbb{C}^{q\times m}$. The matrices $\mathbf{0}_{ij} \in \mathbb{C}^{i\times j}$ correspond to null matrices.

In order to partition the vector of physical fields $\mathbf{w}(z)$ into the state vector $\mathbf{s}(z)$ and the vector of remaining field variables $\mathbf{s}_0(z)$, the system in Eq. (3) may be expressed in terms of non-zero eigenvalues and correspondent eigenvectors. This enables the rewriting of the contributions of the terms in $\mathbf{s}_0(z)$ as a function of the fields in the state vector $\mathbf{s}(z)$. Consequently, the partial derivative of $\mathbf{s}(z)$ with respect to z is obtained as,

$$\frac{\partial}{\partial z}\mathbf{s}(z) = -\left(\mathbf{R}_n\boldsymbol{\Phi}_n\boldsymbol{\Lambda}_n\boldsymbol{\Gamma}_n\mathbf{T}\right)^{-1}\mathbf{R}_n\mathbf{T}\,\mathbf{s}(z), \tag{22}$$

where

$$\mathbf{T} = \begin{bmatrix} \mathbf{I}_n \\ -\mathbf{B}_0{}^{-1}\mathbf{B}_s \end{bmatrix}, \tag{23}$$

and $\mathbf{I}_n \in \mathbb{C}^{n\times n}$ is the identity matrix. The expressions of $\mathbf{B}_0$ and $\mathbf{B}_s$ depend on the non-zero eigenvalues and correspondent eigenvectors. Therefore, the matrix $\boldsymbol{\alpha}$ may be expressed as,

$$\boldsymbol{\alpha} = \left(\boldsymbol{\Gamma}_n\mathbf{A}_z\mathbf{T}\right)^{-1}\boldsymbol{\Gamma}_n\mathbf{R}\mathbf{T}. \tag{24}$$

The details of the semi-analytical derivation of the state matrix for linear homogeneous media may be found in Parra Martinez *et al.*[44]. As may be seen from the latter, this method allows for the derivation of the state matrix for the dynamic analysis of any homogeneous linear media.

II.4 Solution in the eigenspace

The eigenvalue problem associated to $\boldsymbol{\alpha} \in \mathbb{C}^{n\times n}$ reads

$$\boldsymbol{\alpha} = \boldsymbol{\Theta}\, \boldsymbol{\Lambda}_n\, \boldsymbol{\Theta}^{-1}. \tag{25}$$

where $\boldsymbol{\Theta} \in \mathbb{C}^{n\times n}$ and $\boldsymbol{\Lambda}_n \in \mathbb{C}^{n\times n}$ are respectively a matrix whose columns are the eigenvectors, and the diagonal matrix with the eigenvalues. Note that the eigenvalues $\boldsymbol{\Lambda}_n$ correspond to the same eigenvectors as in the un-symmetric eigenvalue problem in Eq. (21), and $\boldsymbol{\Theta}$ correspond to the projection of the n eigenvectors $\boldsymbol{\Phi}_n$ on the n field variables in $\mathbf{s}(z)$. The eigenvalues and eigenvectors represent linearly independent states of motion in the medium, *i.e.* waves: the eigenvalues $\boldsymbol{\Lambda}_n$ are inversely proportional to the wave velocities, and the eigenvectors $\boldsymbol{\Theta}$ represent the polarisation of each wave.

Introducing a change of variables,

$$\mathbf{s}(z) = \boldsymbol{\Theta}\, \mathbf{q}(z) \tag{26}$$

and substituting this into Eq. (7) allows for the solution at a point z to be expressed in terms of the solution at a reference point z_0,

$$\mathbf{q}(z) = \mathbf{e}^{-\boldsymbol{\Lambda}_n\,(z-z_0)}\, \mathbf{q}(z_0), \tag{27}$$

where $\mathbf{q}(z_0) \in \mathbb{C}^n$ is a vector containing the contribution of each wave in the layer at z_0.

Transforming back to physical variables,

$$\mathbf{s}(z) = \boldsymbol{\Theta}\, \mathbf{e}^{-\boldsymbol{\Lambda}_n\,(z-z_0)}\, \boldsymbol{\Theta}^{-1}\, \mathbf{s}(z_0), \tag{28}$$

which describes the wave propagation from z_0 to z in terms of the eigenvectors and eigenvalues of $\boldsymbol{\alpha}$. Therefore, the transfer matrix between the two given points, as expressed in Eq. (8), may be written as

$$\mathbf{M}(z, z_0) = \boldsymbol{\Theta}\, \mathbf{e}^{-\boldsymbol{\Lambda}_n\,(z-z_0)}\, \boldsymbol{\Theta}^{-1}. \tag{29}$$

It follows that

$$\mathbf{s}(z) = \boldsymbol{\Theta}\, \mathbf{L}(z - z_0)\, \mathbf{q}(z_0), \tag{30}$$

where $\left\{\mathbf{L} \in \mathbb{C}^{n\times n},\ \mathbf{L}(z - z_0) = \mathbf{e}^{-\boldsymbol{\Lambda}_n\,(z-z_0)}\right\}$ describes the propagation between z_0 and z.

Consequently, for a medium characterised by a state matrix $\boldsymbol{\alpha} \in \mathbb{C}^{n\times n}$, the solution of the system of equations governing the media can be described as a superposition of n waves in the media.

II.5 Wave properties and dynamic indicators

From a known solution, *i.e.* a point z_0 where the state vector $\mathbf{s}(z_0)$ is known, the wave contributions $\mathbf{q}(z_0)$ can be determined by projecting the corresponding state variables in the eigenspace, as

$$\mathbf{q}(z_0) = \mathbf{\Theta}^{-1}\,\mathbf{s}(z_0). \tag{31}$$

Several wave properties may be derived from the solution in the eigenspace, such as the wave slowness s_i, wave attenuation τ_i, and wavelength λ_i of the i-th wave. Introducing $\imath k_{z,i} = (\Lambda_n)_i$, these can be written as

$$s_i = \mathrm{Re}\left\{\frac{1}{V_i}\right\}, \tag{32}$$

$$\tau_i = -\omega\,\mathrm{Im}\left\{\frac{1}{V_i},\right\}, \tag{33}$$

$$\lambda_i = \mathrm{Re}\left\{\frac{2\pi}{k_{z,i}}\right\}, \tag{34}$$

where $V_i = \omega/k_{z,i}$ is the phase velocity of the i-th wave.

From the state-matrix and the wave space properties, the response may be further assessed in terms of several dynamic and acoustic indicators. For example, the internal powers $\mathcal{P}$ of a material layer of thickness d placed at the origin of a coordinated system, *i.e.* $z_0 = 0$, defined by the integral over the thickness associated with the scalar product of two complex quantities $f(z)$ and $g(z)$ such that $f(z) = \mathbf{T}^f\mathbf{s}(z)$ and $g(z) = \mathbf{T}^g\mathbf{s}(z)$, is expressed analytically as such:

$$\mathcal{P}(f,g) = \int_0^d f^*(z)g(z)\,\mathrm{d}z, \tag{35}$$

where $[^*]$ denotes the complex conjugate operator.

Thus, the integration over the thickness can be rewritten in terms of wave properties and contributions by introducing $\mathbf{\Xi}\{\mathcal{P}\} = \mathbf{T}^{f^*}\mathbf{T}^g$, where the matrix $\mathbf{\Xi} \in \mathbb{C}^{n\times n}$ holds the contribution of the different state variables involved,

$$\mathcal{P}(f,g) = \mathbf{q}^*(0)\left[\int_0^d \mathbf{L}^*(z)\,\mathbf{\Theta}^*\,\mathbf{\Xi}\{\mathcal{P}\}\;\mathbf{\Theta}\,\mathbf{L}(z)\,\mathrm{d}z\right]\mathbf{q}(0). \tag{36}$$

It is important to note that the quadratic factor $\mathbf{\Xi}\{\mathcal{P}\}$ depends on the nature of the quadratic quantity evaluated and the material model.

A similar procedure may be applied in order to obtain the sound transmission loss, sound pressure level, or absorption coefficient of a multilayered system under a plane wave excitation.

Chapter III

Wave propagation in anisotropic poroelastic media

This chapter presents a validation as well as an applications of the proposed method. The validation case of the semi-analytical derivation of the state matrix studies the wave propagation in a poroelastic medium with heavy fluid/solid coupling. Then, a detailed study on the influence of the material orientation on the wave propagation in an anisotropic melamine foam is presented.

As explained by Allard *et al.* [3], the wave properties may be derived by solving the state matrix of the medium for a every material alignment of the medium with respect to the global coordinate system, and then computing the eigenvalue problem, see Eq. (25). The expression of the wave properties in the material or global coordinate system are coupled by trigonometric relations with respect to the material alignment angles.

III.1 Waves in a human femoral bone

The wave propagation in human femoral bone [11] is studied using the semi-analytical derivation of the state matrix. The medium is considered infinite, and modelled using the $\{\mathbf{u}^s, \mathbf{u}^f\}$ representation of the Biot-Newton equations for poroelastic materials under heavy fluid-structure interaction [5,6]. The state of the medium can be described by a set of 6 equations of motion and 7 constitutive laws,

$$\mathbf{0} = \omega^2 \rho\, \mathbf{u}^s + \omega^2 \rho_f \mathbf{u}^f + \nabla \cdot \boldsymbol{\sigma}, \tag{37}$$

$$\mathbf{0} = \omega^2 \rho_f \mathbf{u}^s + \omega^2 \mathbf{Y}\, \mathbf{u}^f - \nabla p, \tag{38}$$

$$\mathbf{0} = \mathbf{C}\boldsymbol{\epsilon} + M\mathbf{a}\nabla \cdot \mathbf{u}^f - \boldsymbol{\sigma}, \tag{39}$$

where (ρ_s, ρ_f, ρ) are respectively the grain density, saturating fluid density, and composite density such that $\rho = (1-\phi)\rho_s + \phi\rho_f$; $\mathbf{u}^s, \mathbf{u}^f \in \mathbb{C}^3$ are respectively the solid and fluid

(relative to the solid) displacements; ϕ is the porosity; p denotes the pore pressure; $\boldsymbol{\sigma}, \boldsymbol{\epsilon} \in \mathbb{C}^6$ are the solid stress and strain vectors; $\mathbf{C} \in \mathbb{C}^{6\times6}$ is the dry-rock stiffness tensor; M denotes the fluid/solid coupling modulus; and $\mathbf{a} \in \mathbb{C}^6$ denotes the vector composed of the effective stress components. $\mathbf{Y} \in \mathbb{C}^{3\times3}$ denotes the Biot visco-dynamic operator defined as

$$\mathbf{Y} = \frac{i\eta_f}{\omega}\,\mathbf{q}_0^{-1} + \frac{\rho_f}{\phi}\,\mathbf{T} \tag{40}$$

where $\mathbf{T}, \mathbf{q}_0 \in \mathbb{C}^{3\times3}$ are respectively the tortuosity and global permeability tensors; and η_f is the dynamic viscosity of the saturating fluid.

For this particular application, an expansion of the form of Eq. (2) is adopted, with a propagation direction such that $k_x = 0$ and $k_y = 0$. Therefore, the vector of field variables $\mathbf{w}(z)$ may be divided into

$$\mathbf{s}_0(z) = \left\{u_x^f(z)\ u_y^f(z)\ \sigma_{xx}(z)\ \sigma_{yy}(z)\ \sigma_{xy}(z)\right\}^{\mathrm{T}}, \tag{41}$$

$$\mathbf{s}(z) = \left\{u_x^s(z)\ u_y^s(z)\ u_z^s(z)\ u_z^f(z)\ \sigma_{zz}(z)\ \sigma_{yz}(z)\ \sigma_{xz}(z)\ p(z)\right\}^{\mathrm{T}}. \tag{42}$$

The system of Eqs. (37)-(39) may be expressed under the form of a simplified linear homogeneous system, see Eq. (3), where $\left\{\mathbf{A}_i \in \mathbb{C}^{13\times13},\ i = \{0, x, y, z\}\right\}$. Their expressions can be found on Appendix A.4.

The expressions of the different material parameters, including the viscoelastic model, may be found in Carcione[11]. The values of the material parameters are detailed in Table 1.

Fig. 1 shows the phase velocities of the waves in the femoral bone. The results are computed, as defined in Sec. II.4, through the post-processing of the state matrix, computed by the semi-analytical method[(i)]. To validate the state matrix formulation and derivation, the results are compared to those computed through the method proposed by Carcione[11].

The solution to the eigenvalue problem consists in four pairs of waves, as predicted by the Biot theory[7,8]. As may be seen from the material parameters in Table 1, the material is modelled as orthotropic, thus its Hooke's law may be described through 9 independent elastic constants. As the eigenvalue problem is computed for all material rotations along the $y-$axis, 3 elastic coefficients remain constant with respect to the rotations, creating two planes of symmetry (xy and yz) in the material parameters. Therefore, only one quadrant of the curves is shown. The velocities of the four waves predicted by Biot[1] may be observed. By studying the polarisation of space in each wave, it can be determined that the two waves with velocities around $2\,\mathrm{km.s^{-1}}$ are quasi-shear (qS) waves. As the solution in terms of waves is calculated for material orientations where the $y-$axis of

[(i)] See Sec. II.3

Human femoral bone

Parameter	Symbol	Value
Water density	ρ_f	$1000\,\mathrm{kg.m^{-3}}$
Water bulk mod.	K_f	$2.5\times10^{9}\,\mathrm{Pa}$
Viscosity	η	$1\,\mathrm{cP}$
Grain density	ρ_s	$1815\,\mathrm{kg.m^{-3}}$
Grain bulk mod.	K_s	$28\times10^{9}\,\mathrm{Pa}$
Porosity	ϕ	1
Tortuosity	$\mathbf{T}$	$\begin{bmatrix} 2 & 0 & 0 \\ & 3 & 0 \\ \text{sym.} & & 3.6 \end{bmatrix}$
Permeability	$\mathbf{q}_0$	$\begin{bmatrix} 1.2 & 0 & 0 \\ & 0.8 & 0 \\ \text{sym.} & & 0.7 \end{bmatrix}\times10^{-12}\,\mathrm{m^2}$
Drained stiffness	$\mathbf{C}$	$\begin{bmatrix} 18 & 9.98 & 10.1 & & & \\ & 20.2 & 10.7 & & 0 & \\ & & 27.6 & & & \\ & & & 6.23 & & \\ & \text{sym.} & & & 5.61 & \\ & & & & & 4.01 \end{bmatrix}\times10^{9}\,\mathrm{Pa}$

TABLE 1. Mechanical parameters of a human femoral bone[11].

the material coordinate system and of the global coordinate system are aligned, one of the qS waves induces exclusively shear deformations (S wave). The other qS wave is polarised in such a way that it also induces compressional deformations on the medium. The two remaining waves correspond to slow and fast quasi-compressional waves (Slow qP and Fast qP).

It may be observed that the two methods yield the same results in terms of eigenvalues to the wave propagation problem in the medium, therefore validating the semi-analytical derivation of the state matrix of the medium.

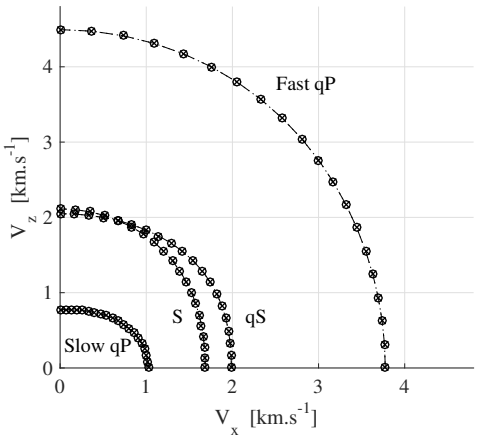

FIGURE 1. Phase velocities of the waves in the xz-plane of a human femoral bone at $f = 10$ kHz. Circled dashed line: method proposed by Carcione[11]. Crossed dotted line: semi-analytical method proposed by Parra Martinez *et al.*[44]

III.2 Waves in an industrial melamine foam

Melamine foam is largely used in several engineering applications due to its low density, and dynamic performances. It is, for example, used for sound absorption in architectural applications, or in the fuselage of aeroplanes. The choice of melamine for the detailed study in this work has been motivated by its known anisotropy. This particular material has been modelled as fully anisotropic and anelastic. The different characterisation techniques that allowed for the derivation of the material parameters here used may be found in the literature[15,16,25,28,31,60–63].

The foam is modelled with the $\{\mathbf{u}^s, \mathbf{u}^t\}$ representation[18] of the Biot theory[7,8], see Eqs. (14)-(17), with a plane wave expansion of the form of Eq. (2), with a propagation direction such that $k_x = 0$ and $k_y = 0$. The state vector is detailed in Eq. (19).

The material parameters are defined in the global coordinate system through the rotation angles $\{\alpha, \beta, \gamma\}$ of the material coordinate system with respect to the global coordinate system[16]. The transformation of tensors are defined through the rotation matrix[16]

$$\mathbf{r} = \mathbf{r}_x(\alpha)\,\mathbf{r}_y(\beta)\,\mathbf{r}_z(\gamma). \tag{43}$$

The flow resistivity of the melamine core at an arbitrary material orientation is given by

$$\boldsymbol{\sigma}^{\text{flow}} = \mathbf{r}\,\boldsymbol{\sigma}_0^{\text{flow}}\,\mathbf{r}^{\text{T}}, \tag{44}$$

with

$$\boldsymbol{\sigma}_0^{\text{flow}} = \begin{bmatrix} 0.9727 & 0 & 0 \\ & 1.0655 & 0 \\ \text{sym.} & & 1.1318 \end{bmatrix} \times 10^4 \text{ Pa.s.m}^{-2}. \tag{45}$$

In a similar way, the stiffness matrix $\mathbf{H}$ is defined at each material alignment[15,16,60] as

$$\mathbf{H} = \mathbf{R}\,\mathbf{H}_0\,\mathbf{R}^{\mathrm{T}}, \tag{46}$$

where $\mathbf{R}$ is the Bond matrix[56] defined by $\mathbf{r}$. The stiffness matrix $\mathbf{H}_0$ is computed from the elastic matrix $\mathbf{C}_0$ through an augmented Hooke's law[16,21,50,61],

$$\mathbf{H}_0 = \mathbf{C}_0 \left(1 + \frac{\hat{b} \left(\frac{\imath\omega}{\hat{\beta}} \right)^{\hat{\alpha}}}{1 + \left(\frac{\imath\omega}{\hat{\beta}} \right)^{\hat{\alpha}}} \right), \tag{47}$$

where $\mathbf{C}_0$ is expressed in the material coordinate system[15,16,60] as

$$\mathbf{C}_0 = \begin{bmatrix} 7.7194 & 3.4252 & -0.0226 & 0 & 0 & 0 \\ & 4.2782 & 1.1845 & 0 & 0 & 0 \\ & & 2.2155 & 0 & 0 & 0 \\ & & & 1.0364 & 0 & 0 \\ & \text{sym.} & & & 1.2368 & 0 \\ & & & & & 1.0123 \end{bmatrix} \times 10^5 \text{ Pa}, \tag{48}$$

and $\hat{\alpha}$, $\hat{\beta}$ and $\hat{b}$ are respectively the fractional derivative order, the relaxation frequency, and the anelastic contribution. The acoustic parameters that derive from the material stiffness and flow resistivity (effective densities, dynamic tortuosity, *etc.*) are then affected by the material orientation. The additional parameters of the melamine foam can be found in Parra Martinez *et al.*[43].

In order to avoid redundancy of rotated states, the angles are then bounded by

$$\alpha \in [-\pi, \pi] \text{ rad}, \quad \beta \in [-\pi/2, \pi/2] \text{ rad}, \quad \gamma \in [-\pi, \pi] \text{ rad}. \tag{49}$$

The rank of the system of Eqs. (14)-(17) is equal to 8. Therefore, as discussed in Chap. II, the solution to the dynamic problem in the medium may be expressed as a superposition of 8 waves.

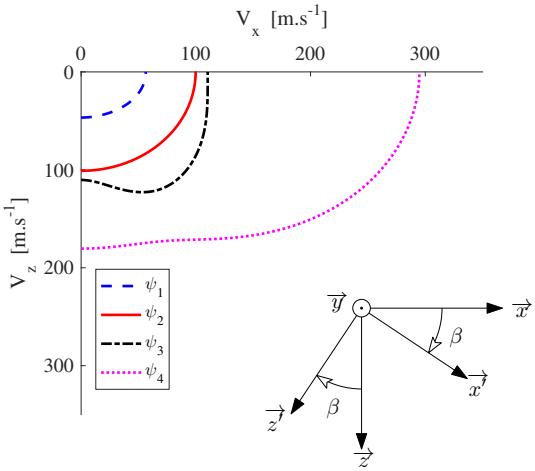

FIGURE 2. Polar representation of the velocities of the waves in an infinite poroelastic anisotropic medium composed of the melamine at $f = 100$ Hz.

Furthermore, the medium is considered infinite in all directions of space. As a consequence of the lack of coupling between the poroelastic medium with any other medium, there are four pairs of waves. Each pair of waves exhibit the same polarisation and velocity, but propagate in opposite travel directions. Note that this is not always the case as, when the poroelastic medium is coupled to other material layers, interactions between the different media at the boundaries affect the wave propagation behaviour[43].

Accordingly, in the following, only the properties of 4 waves are studied, their pairs are omitted.

The velocities of the waves ψ_1, ψ_2, ψ_3 and ψ_4 are shown in Fig. 2 at $f = 100$ Hz in the $xz-$plane. As in the previous section, only one quadrant is shown due to the planes of symmetry induced by the material orthotropy. It may be seen that the velocities of the waves ψ_1, ψ_3 and ψ_4 exhibit a dependence on the material orientation, whereas the wave velocity of the wave ψ_2 is constant in space.

In order to further understand the nature of the acoustic waves, their polarisation in terms of displacement of the solid phase is shown in Fig. 3 for three material orientations. As its velocity, the polarisation of the wave ψ_2 is invariant with respect to the material orientation. Furthermore, its solid displacement polarisation vector is parallel to the $y-$axis of the global coordinate system. This suggests that, due to orthotropy of the material, this wave corresponds to a pure shear wave (S wave).

Moreover, when the material coordinate system is aligned with the global coordinate system ($\beta = 0$ rad, or $\beta = pi/2$ rad), the wave ψ_3 is parallel to the $x-$axis of the global

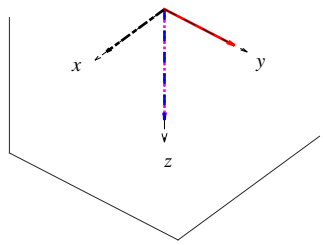

(A) $\beta = 0$ rad

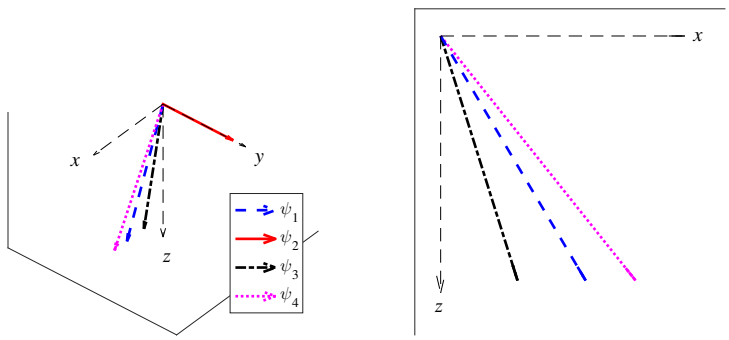

(B) $\beta = \pi/4$ rad

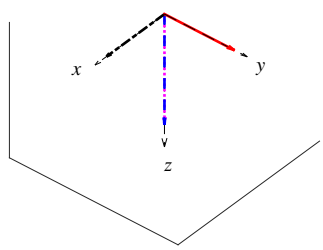

(C) $\beta = \pi/2$ rad

FIGURE 3. Wave polarisations in terms of normalised displacement of the solid phase of the melamine foam at $f = 100$ Hz.

coordinate system, and the waves ψ_1 and ψ_4 are parallel to the $z-$axis. However for any other material orientation, the polarisation of these three waves is in the $xz-$plane, but is not aligned with the global coordinate system. In this particular case of material orthotropy, the wave ψ_3 is known as a quasi-shear (qS) wave, and the waves ψ_1 and ψ_4 correspond to quasi-compressional (qP) waves.

In the case of an arbitrary material orientation, the waves may be polarised an arbitrary direction. Therefore, the nomenclature of the waves in anisotropic media must be defined with respect to criteria other than their polarisation.

Additionally, as discussed by Allard [1], the Biot theory [7,8] identifies the two compressional waves in the poroelastic media as a slow wave and a fast wave.

Nevertheless, it may be seen in Fig. 4a that the velocity of these waves vary strongly with respect to the frequency for a material orientation where $\beta = \pi/2$ rad. At low frequencies, the velocity of the wave ψ_1 is smaller than the velocity of the wave ψ_4. At a frequency close to 750 Hz, the waves exhibit the same velocity. At high frequencies, the velocity of the wave ψ_1 is greater than that of the wave ψ_4. In this case, the velocities of the S and qS waves is constant with respect to the frequency.

Moreover, the Biot theory predicts that, for the case of weak coupling between the saturating fluid and the solid frame (as is the case for the melamine foam) the ratio of fluid to solid displacement tends to 0 for one wave (frame-borne wave) and is higher than 1 for the other wave (airborne wave). This is not the case in the melamine, where the ratio of displacement in the phases is also dependent on frequency, as can be seen in Fig. 4b. As a matter of fact, for frequencies below 750 Hz, both waves are airborne (the ratio of displacement fluid/solid is higher than 1). For higher frequencies, the wave ψ_4 shifts from being predominantly airborne to being predominantly frame-borne. Additionally, it may be seen that both the S and qS waves are frame-borne and the ratio of displacements fluid/solid does not depend on the frequency.

In conclusion, the wave propagation in anisotropic media is strongly dependent of frequency and material orientation, rendering the classification of the waves by velocity or polarisation in space inappropriate.

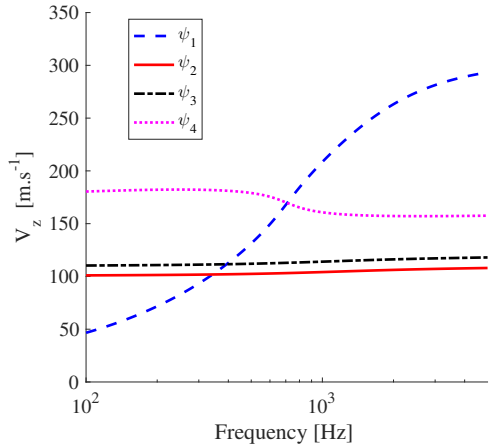

(A) Velocities

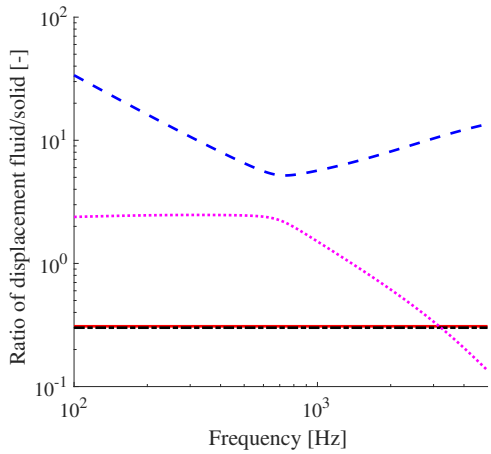

(B) Ratio of displacement fluid/solid

FIGURE 4. Wave properties in an infinite poroelastic anisotropic medium composed of the melamine for $\beta = \pi/2$ rad.

Chapter IV

Dynamics of multilayered systems with anisotropic poroelastic media

In this chapter, the proposed method is used to study the influence of the anisotropy of poroelastic media in the dynamic behaviour of a multilayered panels including such media. Additionally, an optimisation problem is solved to investigate the potential acoustic performance enhancement of a panel by manipulating the orientation of one or two independently aligned identical anisotropic poroelastic core layers.

IV.1 Influence of the material orientation of anisotropic poroelastic cores in multilayered systems

A multilayered system, as seen in Fig. 5, is studied. The core is made of an 88mm anisotropic visco-elastic porous melamine foam. The face sheets are composed of 1mm isotropic solid aluminium. The material parameters of the different layers can be found in Parra Martinez *et al.* [43].

Three study types of harmonic acoustic excitation are considered: normal incidence ($\theta_1 = \theta_2 = 0°$), oblique incidence ($\theta_1 = 45°, \theta_2 = 50°$), and diffuse field. The latter corresponds to a superposition of plane waves with incidence angles ranging from 0° to 70° for the altitude angle, and from 0° to 360° for the azimuth angle. The angles are distributed according to Gauss-Legendre quadratures. The number of points was chosen through a preliminary convergence study of the solution. It was determined that using 12 points for the azimuth distribution, and 12 points for the altitude distribution were sufficient to model the acoustic diffuse field.

The melamine is modelled with the $\{\mathbf{u}^s, \mathbf{u}^t\}$ representation [18] of the Biot theory [7,8], as defined in Eqs. (14)-(17). The state vector of the medium is detailed in Eq. (19). The influence of the anisotropy of the core is studied by successive rotations of the

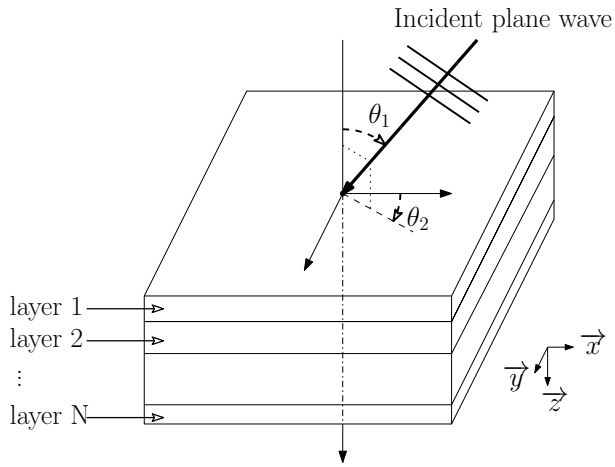

FIGURE 5. Multilayered system studied under plane wave incidence.

material coordinate system of the melamine with respect to the global coordinate system, as defined in Eq. (43). The state matrix of each layer, as well as the solution to the dynamic problem, were computed with the method in Chap II. A comparison is made with a configuration in which the anisotropic core is replaced with its closest isotropic equivalent poroelastic core, here computed through a method proposed by Norris[40].

IV.1.1 Dynamic behaviour

A preliminary study on the influence of the rotations through transformations with respect to one single rotation angle was performed. It was found[45] that the rotations with respects to the $y-$axis of the material coordinate system, *i.e.* defined by the angle β, had a greater influence on the response of the structure than the rotations with respect to the $x-$ or $z-$axes. Therefore, in the following, only the influence with respect to rotations of the material coordinate system around the $y-$axis is presented.

Fig. 6 presents the sound transmission loss (STL) of the multilayered system under a normally incident, obliquely incident, and diffuse field excitations as a function of the frequency, defined as,

$$\mathrm{STL}(f) = -10 \log \left| \frac{W_r(f)}{W_i(f)} \right|, \tag{50}$$

where W_r and W_i are respectively the sound power incident on the structure, and the sound power radiated by the bottom face sheet of the structure.

Under all incidence cases, the lower frequency behaviour ($f \lesssim 800$ Hz) is characterised by a shift in the fundamental resonance frequency. This resonance frequency shift translates into STL differences of up to ~ 15 dB between two core material orientations.

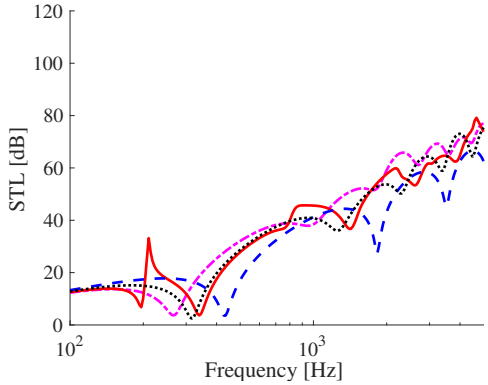

(A) Normal incidence

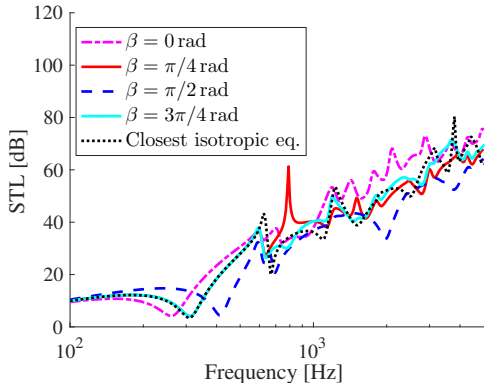

(B) Oblique incidence

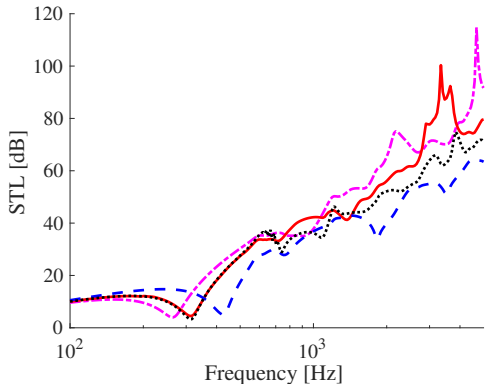

(C) Diffuse field

FIGURE 6. STL of the multilayered system.

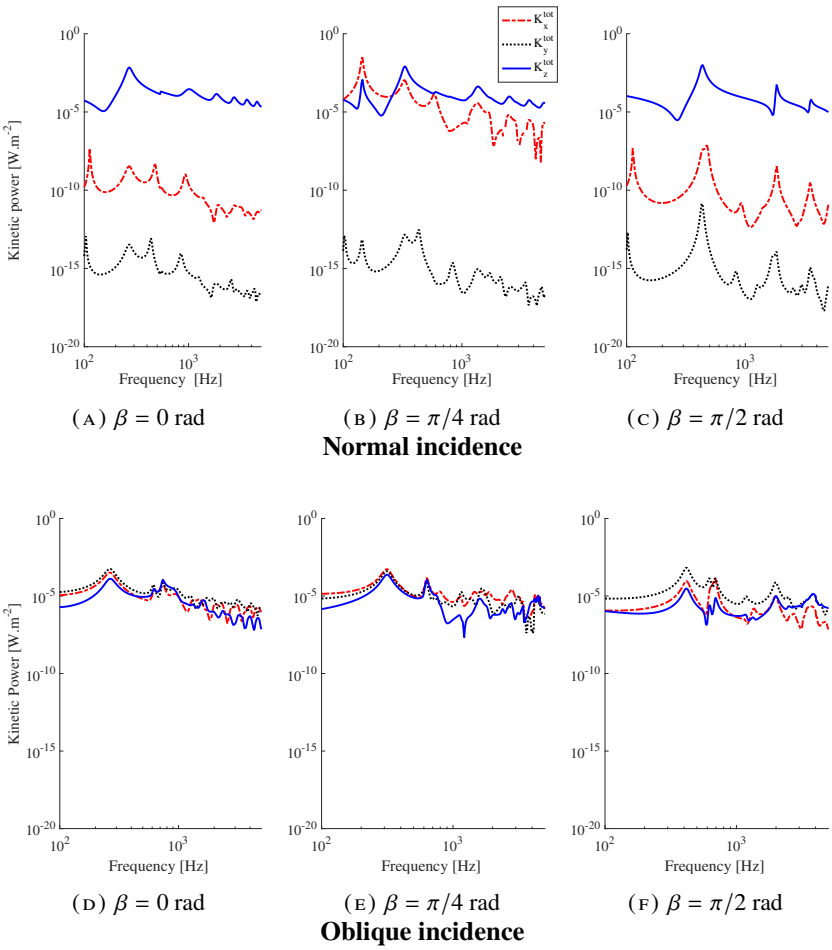

(A) $\beta = 0$ rad (B) $\beta = \pi/4$ rad (C) $\beta = \pi/2$ rad

Normal incidence

(D) $\beta = 0$ rad (E) $\beta = \pi/4$ rad (F) $\beta = \pi/2$ rad

Oblique incidence

FIGURE 7. Kinetic power of the poroelastic core.

Noticeably, under normal incidence, the configuration where $\beta = \pi/4$ rad presents a resonance and anti-resonance at $f \sim 145$ Hz, which is not apparent in other rotations or under other excitations, that translate into a difference of STL of $\sim$ 20dB.

In higher frequencies ($f \gtrsim 800$ Hz), for alignments where $\beta \sim \pi/2$ rad, the response is characterised a more resonant behaviour than for other material orientations. However, the appearance of anti-resonances affect the response of the panel for particular frequencies, increasing the STL of $\sim$ 50 dB between two configurations in some cases.

The influence of the material alignment on the acoustic behaviour of the system is also observed in the kinetic power associated with the motion in the core, as seen in Fig. 7. The partitioning of the kinetic power into the contributions due to motions in the $x-$,

$y-$ and $z-$directions illustrates the nature of the deformations induced by the excitation. It is important to note that the kinetic power associated with the motion in one particular direction does not imply that the core deforms in a particular way.

Under normal incidence, the kinetic power associated with the motion in the $z-$direction is several orders of magnitude higher than the kinetic power associated with the motions in x and y over all of the frequency range. As the material orientation tends to $\beta = \pi/2$ rad, the kinetic power associated with the motion in z is more resonant than for other material alignments. This correlates with the resonant profile of the STL at higher frequencies, as seen in Fig. 6a. However, when $\beta = \pi/4$ rad, the kinetic power associated with the motion in x-direction is higher than the kinetic power associated with the motions in y and z at very low frequencies. For the same material alignment, an anti-resonant behaviour may be observed at $f \sim 145$ Hz. This suggests that, by correlation with the STL, see Fig. 6a, there is a change in the nature of the deformations induced in the core by the material orientation around that particular frequency, that directly affects the acoustic performance of the panel.

Under oblique incidence, the kinetic powers associated with motions in all directions have a similar order of magnitude for all material orientations. This suggests that the deformations of the core are strongly linked with the angle of incidence of the excitation.

Similarly, under an acoustic diffuse field excitation, see Fig. 3 in Parra *et al.*[46], the kinetic powers are similar for all material orientations. The kinetic power associated with motion of the core in the $z-$direction is higher in low frequencies than the power associated with motions in the other directions. At certain frequencies, the power associated with motions in the x-direction is more important, suggesting a change in the nature of the motion governing the behaviour of the core at those frequencies. These will be discussed more depth in the following.

IV.1.2 Phenomena intrinsic to the influence of anisotropic poroelastic media in multilayered systems

In particular, two phenomena may be observed from the dynamic response of the studied multilayered system.

IV.1.2.1 Fundamental resonance frequency shift

The fundamental resonance is commonly known as the mass-spring-mass resonance of the multilayered system[22]. In multilayered systems where the core is modelled as isotropic, the frequency at which this resonance occurs is proportional to the square root of the Young's modulus of the poroelastic core. However, when the core is anisotropic, the

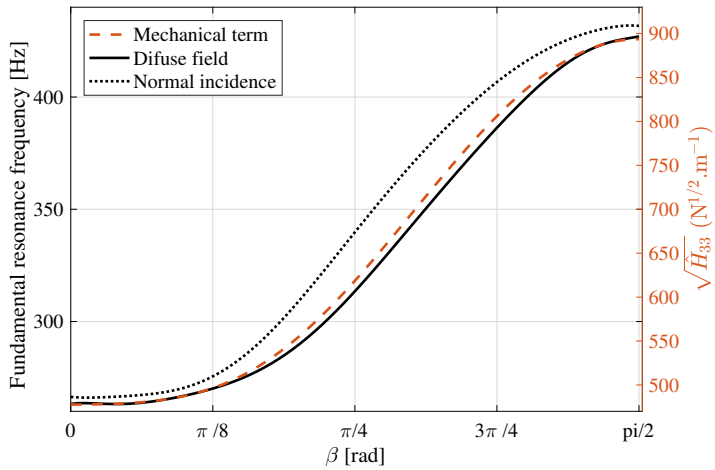

FIGURE 8. Fundamental resonance of the multilayered system under normally incident and diffuse field excitations, and stiffness coefficient $\sqrt{H_{zz}}$ as a function of the material alignment rotation.

value of the stiffness coefficients in the Hooke's matrix depend on the material orientation. As seen in the STL and kinetic powers, the fundamental resonance of the panel shifts in frequency when the material orientation changes. The fundamental resonance frequency as a function of the core material orientation is shown in Fig. 8. There is a correlation between the stiffness in compression along the $z-$axis of the poroelastic core and the frequency at which the fundamental resonance occurs. Furthermore, the correlation between resonance frequency and stiffness in compression is higher when the system is excited by a diffuse field, but is however not constant with respect to the material alignment angle. This suggests that the panel does not exhibit only a compressional deformation at the fundamental resonance, but rather a superposition of compressional and shear deformations.

IV.1.2.2 Compression-shear coupling

The material core model in this application corresponds to an orthotropic medium, as described by Cuenca *et al.* [16] and Van der Kelen *et al.* [60]. When the material coordinate system is not aligned with the global coordinate system, the stiffness matrix **H** of the core, see Eq. (48), presents only compression-compression (known as Poisson effect), and shear terms. As the material coordinate system is rotated, compression-shear coupling terms appear in the matrix. This suggests that the response of the core will present

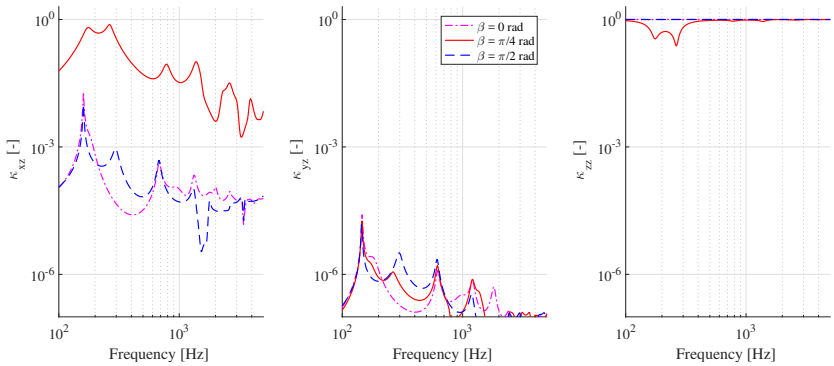

FIGURE 9. Relative deformation of the solid frame of the poroelastic core in the $xz-$ and $zz-$ planes, according to Eq. (51), under normally incident plane wave excitation of the panel. The relative deformation in the $yz-$plane is negligible in this case.

couplings between compressional and shear deformations, regardless of the type of traction excitation applied to the core.

The effects of the compression-shear coupling in the poroelastic core are mainly visible under normally incident excitation. This is due to the fact that, under this particular excitation case, the top face sheet of the panel only exerts a compressional stress on the poroelastic core.

For rotations where the material orientation tends to be aligned with the global coordinate system, *i.e.* $\beta \sim 0$ rad and $\beta \sim \pi/2$ rad, the waves governing the power transmission through the medium are pure compressional. In contrast, for $\beta \sim \pi/4$ rad, the contributing waves exhibit a high shear deformation, reflecting a high degree of compression-shear coupling. As may be seen in Figs. 6a and 7b, a consequence of this coupling is that a resonance/anti-resonance appears at low frequencies ($f \sim 145$ Hz). Fig. 9 shows the relative deformation along the $z-$axis in the solid phase of the poroelastic core at $f \sim 145$ Hz. The resulting deformation is expressed as a sum of the n waves in the layer ($n = 1 \ldots, 8$ in poroelastic media under the Biot representation) at the frequency f, and is defined as

$$\kappa_{rz}(f) = \frac{\sum_{n=1}^{8} \left| \left[\epsilon^s_{rz}(f) \right]_n \right|}{\sum_{k,l=x,y,z} \left\{ \sum_{n=1}^{8} \left| \left[\epsilon^s_{kl}(f) \right]_n \right| \right\}}, \qquad \text{for } r = x, y, z, \tag{51}$$

where $\epsilon^s_{kl} = \frac{1}{2}\left(\frac{\partial u^s_k}{\partial l} + \frac{\partial u^s_l}{\partial k} \right)$ for $k, l = x, y, z$. It may be seen that the excitation induces an overall compressional deformation along the $z-$direction. For core material orientations

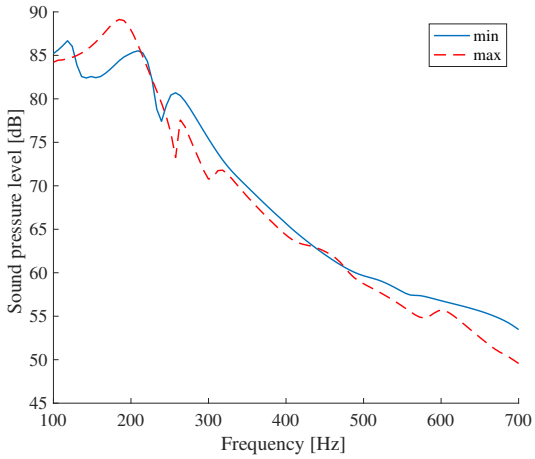

FIGURE 10. Sound pressure level spectra for maximum and minimum solutions of the optimisation problem defined by Lind Nordgren *et al.* [34], computed with the method proposed in Chap. II.

where $\beta = \pi/4$ rad, the behaviour of the material is governed by a shear deformation for frequencies close to $f \sim 145$ Hz.

In conclusion, there is a strong influence of the core material orientation in the dynamic behaviour of multilayered systems composed of anisotropic poroelastic cores. Whether this may be used to enhance the acoustic performance of multilayered panels is explored in the following.

IV.2 Optimal alignment of anisotropic poroelastic cores in a multilayered system for dynamic performances

In a recent paper, Lind Nordgren *et al.* [34] showed that the response of a sandwich panel could be optimised for vibro-acoustic performance by manipulating the material orientation of two anisotropic poroelastic cores in the structure. The panel corresponds to two solid face sheets separated by two independently oriented orthotropic poroelastic foams and a thin air gap. Fig. 10 shows the sound level spectra of the panel configurations in the optimal material orientations, computed through the method proposed in Chap. II. Even though there is a difference in amplitude and frequency with respect to the results in Lind Nordgren's publication, the optimal solution spectra computed by the two methods exhibit the same global trends. The discrepancies arise from the difference in modelling techniques. Indeed, Lind Nordgren *et al.* modelled a finite sized panel under a local

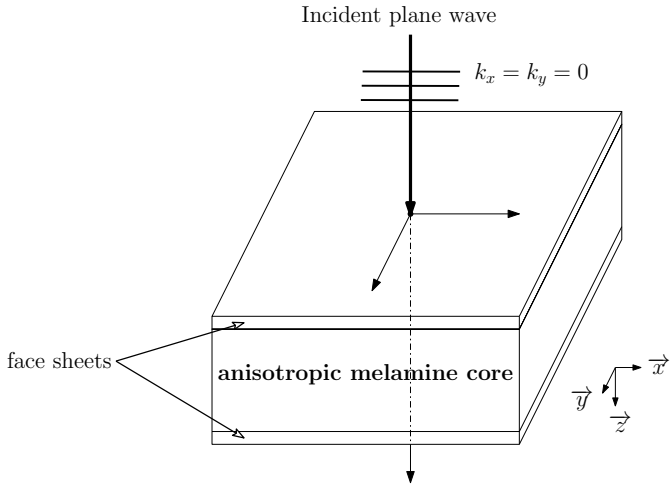

FIGURE 11. Multilayered system setup used in the optimisation problems.

harmonic excitation source, evaluating the radiated pressure by integrating the pressure field a finite volume on a radiated fluid volume. The results shown in Fig. 10 represent the computation of the solution of an infinite panel under diffuse field excitation. Lind Nordgren found that the fundamental resonance frequency and amplitude of a sandwich panel with two identical anisotropic poroelastic cores could be controlled by manipulating the material alignment of the cores. However, the extreme points were not studied in terms of physical phenomena taking place within the material layers.

In order to understand the physical phenomena governing the behaviour of the structure at the optimal solutions, an alternative optimisation problem is defined.

IV.2.1 Multilayered system and design variables

The studied setup is shown Fig. 11. The dimensions of the layers and materials used represent structures commonly used in aeronautical and vehicle engineering applications. The panel consists of an orthotropic melamine core of 88mm in between two isotropic aluminium face sheets[(i)].

An acoustic performance indicator F is constructed in terms of the STL of the panel, as defined in Eq. (50), under a normally incidence acoustic wave excitation of frequency f. It is defined as the sum of the STL over a frequency range discretised by a resolution Δf,

$$\mathrm{F} = \sum_n \{\mathrm{STL}(f_n)\} \,. \tag{52}$$

[(i)]The material parameters may be found in the appended publications [43].

The optimisation problem is solved with the GCMMA algorithm[57,58]. The gradients of the solution at each iteration are calculated through finite differencing.

The design variables are the Tait-Bryan rotation angles $\{\alpha, \beta, \gamma\}$ of the poroelastic core material coordinate system with respect to the global coordinate system[16].

In order to understand the physical phenomena dominating the behaviour of the core at the optimal configurations, two systems are studied. The two configurations of panels, referred to as the one-core system and the two-core system, correspond to the panel defined in Fig. 11, composed respectively of one or two core layers independently oriented. In both configurations, the thickness of the panel is 88mm, which means that each core in the two-core system is 44mm thick.

The design space for the one-core system is defined by the variables $\{\alpha, \beta, \gamma\}$. The design variables of the two-core system is defined by the variables $\{\alpha_t, \beta_t, \gamma_t, \alpha_b, \beta_b, \gamma_b\}$, where t and b refer to respectively the top and bottom core layers.

IV.2.2 Optimisation problem and stability of extreme points

The optimisation problems for the one-core and two-core systems are respectively

$$\begin{aligned}
&\underset{\mathbf{x}}{\text{opt.}} \quad \mathrm{F}(\mathbf{x}) && \text{and} && \underset{\mathbf{x}}{\text{opt.}} \quad \mathrm{F}(\mathbf{x}) \\
&\text{s.t.} \quad \mathbf{x} = \{\alpha, \beta, \gamma\}, && && \text{s.t.} \quad \mathbf{x} = \{\alpha_t, \beta_t, \gamma_t, \alpha_b, \beta_b, \gamma_b\}, \\
&\qquad \alpha \in [-180^\circ, 180^\circ], && && \qquad \alpha_t, \alpha_b \in [-180^\circ, 180^\circ], \\
&\qquad \beta \in [-90^\circ, 90^\circ], && && \qquad \beta_t, \beta_b \in [-90^\circ, 90^\circ], \\
&\qquad \gamma \in [-180^\circ, 180^\circ], && && \qquad \gamma_t, \gamma_b \in [-180^\circ, 180^\circ],
\end{aligned} \tag{53}$$

where 'opt.' denotes minimisation or maximisation. The design variables at optimal solution are denoted $\mathbf{x}^*$. The cost function at the optimal point defined by $\mathbf{x}^*$ is denoted $\mathrm{F}(\mathbf{x}^*)$.

As a measure of robustness of the solution in terms of sensitivity with respect to the design variables, a stability indicator δ of the solution is defined as

$$\delta^{\mathrm{F}}(\mathbf{x}^*) = \frac{\max\limits_{\mathbf{x}} \left\{ \left| \dfrac{\partial \mathrm{F}(\mathbf{x}^*)}{\partial \mathbf{x}} \right| \right\}}{|\mathrm{F}(\mathbf{x}^*)|}, \tag{54}$$

whit $x_{\text{stab}} = \underset{\mathbf{x}}{\text{argmax}} \left\{ \left| \dfrac{\partial \mathrm{F}(\mathbf{x}^*)}{\partial \mathbf{x}} \right| \right\}$.

The solution is stable, or robust, when $\delta \to 0$, *i.e.* when its sensitivity to a small variation of the design variable x_{stab} is small. Correspondingly, the solution is unstable

when $\delta \to \infty$, which means that a small variation of the design variable x_{stab} would strongly affect the value of the cost function.

In the current work, a number of different randomly chosen starting points were used within the design space. However, the complex phenomena governing the dynamic behaviour of the multilayered system render the chosen cost function F non-convex in the design space. Thus, there is no natural global optimal solution, rather local extreme points (maxima and minima). In particular, the strong frequency dependence together with the occurrence of local system resonances in the spectrum, are factors contributing to this aspect. Therefore, a criterion based on Pareto optimality[38] was defined as a function of the value of the cost function at the solution and the robustness of the solution. The optimal design variables of the Pareto solution are denoted $\mathbf{x^P}$, and the cost function at the point defined by $\mathbf{x^P}$ is denoted $\mathrm{F_P}$.

In the following, unless indicated, only the Pareto optimal solution of each system optimisation is addressed.

IV.2.3 Short-range frequency optimisation for acoustic performance

A first range of frequency is studied, chosen in order to capture both the fundamental resonance frequency shift and compression-shear coupling effects observed in Chap. III. The frequency range is defined as $f = [100 - 600]$ Hz.

The STL of the panel at $\mathbf{x^P}$ may be found in Fig. 12 for the minimisation and maximisation of F. It shows that the minimisation of the one- and two-core systems converge to solutions with the same acoustic response. On the other hand, the maximisations converge to solutions with different acoustic behaviour. This suggests that the acoustic response of the overall system may be improved by partitioning the core into two layers of equal thickness with individual material orientations.

The real part of the stiffness coefficients $\mathbf{H}_{35}$, $\mathbf{H}_{34}$ and $\mathbf{H}_{33}$ (respectively $\mathbf{H}_{xz}$, $\mathbf{H}_{yz}$ and $\mathbf{H}_{zz}$) at 40 different solutions $\mathbf{x}^*$ are shown in Fig. 13. These coefficients relate the compressional stress σ^s_{zz} and the strains ϵ^s_{xz}, ϵ^s_{yz} and ϵ^s_{zz}. It can be seen that the minimisations yield solutions where the core layers exhibit a high compressional stiffness and a negligible shear stiffness. The maximisations converge to solutions where the core layers have a low stiffness in compression. However, the solutions to the one-core system maximisation present a negligible stiffness in shear. In contrast, in the solutions to the two-core system maximisation, the core layers are oriented in such a way that there is a non-negligible shear stiffness. This shear stiffness difference between the solutions of the one- and the two-core systems maximisations explains the difference in the STL at the Pareto optima, see Fig. 12b.

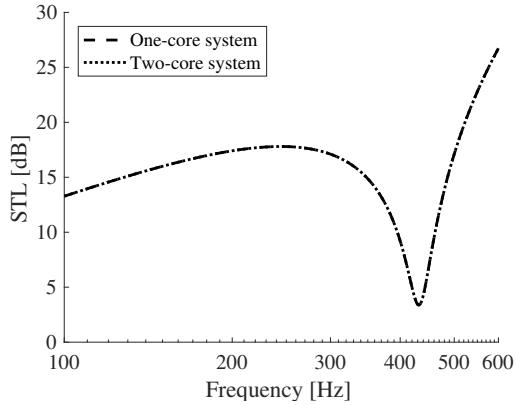

(A) Minimisations.

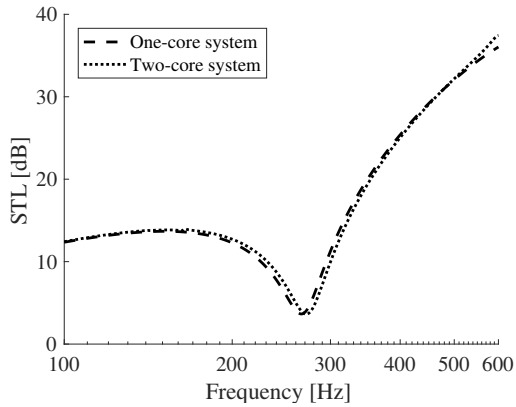

(B) Maximisations.

FIGURE 12. STL at the Pareto optimal solutions of the optimisation problems in Eq. (53).

One phenomenon that is not observed under the presented optimisation setup, which was observed by Lind Nordgren *et al.* [34], is the amplitude variation of the fundamental resonance. The reason might be the difference between the system modelled, which do not capture the same physics governing the fundamental resonance of the panel. As seen in Sec. IV.1.2.1, the deformations responsible for the fundamental resonance in multilayered systems including anisotropic poroelastic cores are not exclusively compressional. The system modelled by Lind Nordgren includes an air gap, mechanically decoupling the bottom core layer and the radiating face sheet. The air gap ensures that only compressional stresses are applied from the bottom core layer to the air gap, and consequently to the bottom face sheet. In the system modelled in the current work, the bottom core layer

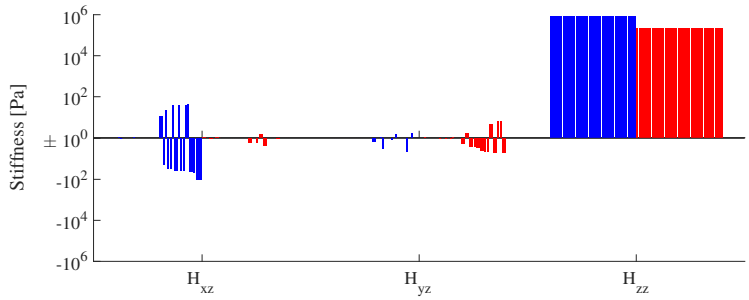

(A) One-core system

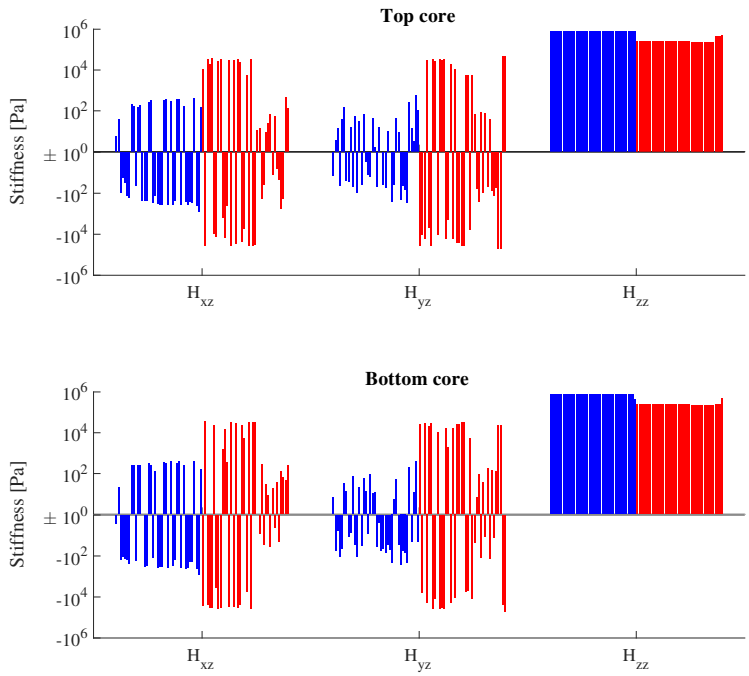

(B) Two-core system

FIGURE 13. Real part of the stiffness coefficients $\mathbf{H}_{35}$, $\mathbf{H}_{34}$ and $\mathbf{H}_{33}$ of the poroelastic material core layers at $\mathbf{x}^*$. Legend: minimisations in blue, maximisations in red.

is perfectly bounded to the radiating face sheet. Thus, there is a continuity of stresses normal to the interface between the two layers. Both compressional and shear stresses are then applied to the radiating face sheet. As a consequence, the deformations inducing

the fundamental resonance of the system are not the same when the system includes an air gap.

IV.2.4 Large-range frequency optimisation for acoustic performance

A second range of frequencies, $f = [100 - 1100]$ Hz, allows to isolate the effects induced by the mechanical anisotropy of the core, disregarding the high-frequency acoustic effects induced by the anisotropy of the flow resistivity[45].

All of the solutions $\mathbf{x}^*$ to the minimisation problem, each from a random ensemble of starting points within the design space, lead to the same cost function acoustic response. Furthermore, all the extreme points found share a material alignment yielding the same stiffness in compression in the $z-$direction in the core, represented by the term $\mathbf{H}_{33}$ of the Hooke's law of the poroelastic layers, *i.e.* $\mathbf{H}_{33} = 8.074 \times 10^5(\pm 10^{-9})$ Pa. This corresponds to material alignments where the melamine layer is the stiffest in compression, thus shifting the fundamental resonance frequency to high frequencies[43]. These results, as well as the short-frequency range minimisations, suggest that the system might present a global minimum acoustic performance with regards to the cost function F.

The relative deformation in the poroelastic core(s) for the solution to the maximisation problem shows that the motion in the core is governed by compression strain on the $z-$axis. However, it presents a significant shear deformation on both $xz-$ and $yz-$planes, which, for some particular frequencies in the low-frequency domain, govern the mechanical response of the core. Furthermore, the compressional deformation in the $z-$axis of the two poroelastic layers in the two-core system governs the overall behaviour of the core, and present a significant shear deformation for some particular frequencies. Also, it may be observed that the top core of the two-core system behaves like the core of the one-core system. The shear deformation of the bottom core layer dominates the behaviour of the core at a higher frequency rage.

Note that the system is excited by a normally incident plane wave, inducing exclusively a traction on the $z-$direction on the top face sheet. Consequently, the solution to the maximisation problem is one which takes advantage of the STL improvement induced by shear-compression coupling effects in the poroelastic cores.

To explore this further, an alternative cost function may be constructed from the relative shear deformations, defining a new maximisation problem,

$$\max_{\mathbf{x}} \quad \mathrm{S}(\mathbf{x}) = \sum_n \sum_c \left\{ \kappa^c_{xz}(f_n, \mathbf{x}) + \kappa^c_{yz}(f_n, \mathbf{x}) \right\} \tag{55}$$

where κ is the relative deformation, see Eq. (51); c is the number of layers of equal thickness which are composing core; and $\mathbf{x}$ is the design variables of the one-core or two-core systems. The design variables and design space remain the same as in the optimisation of acoustic performances. In this case, the stability indicator is defined as in Eq. (54) with respect to S.

The solutions to the maximisation of S show a similar relative deformation profile in the core(s) as in the case of maximisation of F. The one-core system exhibits a significant amount of shear deformation which governs the mechanical behaviour of the core at lower frequencies. The solution to the two-core system maximisation presents a particular dependence on the frequency. The top core is oriented as the core in the one-core system solution, inducing similar relative deformations. In contrast, the bottom core is oriented in such a way that the shear deformation on high frequencies is significant.

The acoustic response of the panel at the solutions to the different optimisation problems show that the maximisation of F and of S lead to solutions where the STL exhibits different shear-compression coupling resonance frequencies, as well as a different behaviour in high frequency. This high frequency difference in STL directly correlates to the shear induced by the bottom core in the two-core system.

It may be seen that the solutions to the maximisation of F and of S are not the same. However, the optimisation of S may be used for the tuning of the resonances and anti-resonances in the system, improving the STL of the system at particular frequencies.

Chapter V

Conclusions

The central subject of this thesis is the study of wave propagation and dynamic analysis of multilayered systems, and, in particular, those including anisotropic poroelastic media. Among the main outcomes of the thesis is a method for the semi-analytical derivation of the full solution of multilayered panels including anisotropic poroelastic materials. The method provides insight in the physical mechanisms governing energy transmission and dissipation in the media. Important results have been achieved by using the developed method as a design tool. In particular, and most interestingly, it has been shown that the sound transmission loss of a multilayer panel may be enhanced, without an increase in its mass or volume, by partitioning a poroelastic layer into two sub-layers with independent material orientation.

The proposed method for the study of multilayered systems is based on the expansion of the dynamic solution as a superposition of plane waves. The formulation relies on a state-space representation in terms of physical field variables, and directly provides the characteristics of the waves in the different layers of the structure. The state-space representation requires the computation of the state matrix, characterising the dynamic state of each material layer in a system. Two methods for the derivation of the state matrix have been studied. A *term-by-term*, or analytical derivation, has been presented for the acoustic analysis of fluid (or fluid equivalent), solid, and poroelastic media. However, it has been proven to being unpractical and prone to errors for media where the state vector is large. Consequently, a semi-analytical derivation method of the state matrix has been derived. Given its formulation, the state matrix of any type of linear homogeneous medium, including arbitrary anisotropic properties and multi-physics interactions, may be implemented.

Using the proposed method, a study of the wave propagation in anisotropic poroelastic media has been performed. The validation of the state matrix derivation method has been done. By computing the eigenvalues to the wave propagation problem in a poroelastic

medium with strong fluid/solid dynamic coupling, the proposed method was validated against a model available in the literature. Additionally, the analysis of the wave propagation in an industrial anisotropic melamine foam was presented. It was found that, for this commonly used material, there is a strong influence of the inherent anisotropy of the material in the wave propagation through the medium.

Having established the effects of the anisotropy on the wave propagation through the medium, the influence of the anisotropy of poroelastic cores on the dynamic behaviour of multilayered systems, as well as the phenomena within the material layers, has been evaluated. By varying the material orientation of the anisotropic poroelastic core in a multilayered system, it was found that the core alignment had a strong influence on the wave propagation in the medium, as well as on the acoustic behaviour of the panel. A shift in the fundamental resonance frequency of the overall structure is observed, and may be linked to the variation of the stiffness coefficient linking traction to compressional strains within the core medium with respect to its orientation. Furthermore, the shear-compressional effects have been shown to have an important influence on the behaviour of the structure.

Finally, an optimisation problem for acoustic performance has been studied in terms of material orientation of the anisotropic poroelastic cores of a multilayered system. The optimal solution was obtained through a Pareto optimality criterion. The latter was constructed from the value of the cost function of the solution, and the robustness of the solution in terms of sensitivity to small variations in the design variables. It was found that the system exhibits a global minimum, regardless of the number of layers in which the core is partitioned. This was correlated to the stiffness in compression of the poroelastic core at the solution for each layer. Moreover, it was shown that the acoustic response of a multilayered system in terms of sound transmission loss could be improved by sectioning the core into two independently oriented poroelastic layers, without increasing the mass of the overall system. The improvement of sound transmission loss was correlated to the dynamic phenomena in the core layers. Based of these results, an alternative optimisation problem was defined in terms of shear-compression coupling. The solution was found to differ in terms of overall acoustic performance, but may be exploited for the tuning of the acoustic behaviour at particular frequencies.

Quo vadis?

The methods and results in this thesis open several possibilities for expansion.

The state matrix semi-analytical derivation has been developed in such a way that the only input are the matrices proportional to the partial derivatives. In this thesis, the

state matrix was computed for acoustic problems. It would be then interesting to extend the algorithm with sets of linear equations that combine different types of physics. The question that arises is how to evaluate the interaction between such physics within a medium. This is of particular interest in geophysical applications, where phenomena such as electrosiesmic waves are subjected to multi-physical modelling [12,49].

Another motivating subject of studies that would profit of such developments is the influence of temperature gradients on the dynamic and acoustic behaviour of multilayered structures. Recent studies have shown that there is an influence of temperature gradients in open-celled foams in their mechanical parameters [31]. It is then of interest to study the phenomena induced by temperature gradients in the different layers, and how it affects the transmission of acoustic power through the system.

Furthermore, the studied structures are modelled as infinite in two directions. Some studies have been done with respect of the inclusion of effects inherent to finite-sized structures (like boundary effects) on in-plane infinite models by multiplying the radiation efficiency of the structure by a corrective factor [1] but present limitations with respect to the systems with complex geometries. It is then of interest to adapt the method presented in this thesis to the modelling of finite-sized structure, by coupling the derivation to finite-sized methods, such as the finite-element method [30], or the wave based method [20].

Finally, the method presented in this thesis with respect to the dynamic analysis of multilayered systems have been partially validated with respect to other existing models in the literature. It is however of interest to develop experimental validating techniques, where the poroelastic material core is manufactured with controlled anisotropy and material orientation. An option is to look into the development of advanced manufacturing techniques, such as 3D-printing, for the realisation of microscopically controlled geometric cells, amounting to a controlled macroscopic anisotropy of the material.

Chapter A

Matrices for the semi-analytical calculation of the state matrix in linear homogeneous media

In the following, the matrix $\mathbf{I}_n$ correspond to the identity matrix of dimensions $n \times n$. The matrix $\mathbf{A}_0$ corresponds to the sum of the matrices $\mathbf{A}_a$ and $\mathbf{A}_b$. A numerical convention is used for the referencing of explicit rows and columns in tensors. For a given first or second order tensor $\mathbf{f}$, in the notation $\mathbf{f}|_{i:j}^{k:l}$ the subscripts refer to the lines i to j, and the superscripts refer to the columns k to l. The stand-alone symbol [:] corresponds to all the elements in a corresponding dimension. An integer alone corresponds to the index of an individual row (or column).

A.1 Fluid (or fluid equivalent) media

The dimensions of the matrices are $\left\{\mathbf{A}_i \in \mathbb{C}^{4\times4},\ i = \{a, b, x, y, z\}\right\}$. The state vector is detailed in Eq. (6).

$$\mathbf{A}_a|_i^j = \begin{cases} 1 & i = 4,\ j = 4, \\ 0 & \text{otherwise} \end{cases} \tag{56}$$

$$\mathbf{A}_b|_i^j, = \begin{cases} -\imath\omega\rho_f \mathbf{I}_3 & i = 1, \ldots, 3,\ j = 1, \ldots, 3, \\ 0 & \text{otherwise.} \end{cases} \tag{57}$$

$$\mathbf{A}_x|_i^j = \begin{cases} -1 & i = 1,\ j = 4, \\ K_f & i = 4,\ j = 1, \\ 0 & \text{otherwise.} \end{cases} \tag{58}$$

$$\mathbf{A}_y\big|_i^j = \begin{cases} -1 & i = 2,\ j = 4, \\ K_f & i = 4,\ j = 2, \\ 0 & \text{otherwise.} \end{cases} \tag{59}$$

$$\mathbf{A}_z\big|_i^j = \begin{cases} -1 & i = 3,\ j = 4, \\ K_f & i = 4,\ j = 3, \\ 0 & \text{otherwise.} \end{cases} \tag{60}$$

A.2 Solid elastic media

The linear dynamic state of a solid elastic medium may be described through 6 constitutive laws (Hooke's law) and 3 equations of motion, respectively

$$\boldsymbol{\sigma} = \mathbf{C}^e\, \boldsymbol{\epsilon}, \tag{61}$$

$$\nabla \cdot \boldsymbol{\sigma} = -\omega^2 \rho_s \mathbf{u}^e, \tag{62}$$

where $\mathbf{u}^e$, is the vector of displacement fields; $\boldsymbol{\epsilon}$ and $\boldsymbol{\sigma}$ are the solid Cauchy strain and stress vectors, related by the stiffness matrix $\mathbf{C}^e \in \mathbb{C}^{6\times6}$; and ρ_s is the density of the solid. The state vector and redundant field variables vector are respectively

$$\mathbf{s}(z) = \left\{u_x(z)\ u_y(z)\ u_z(z)\ \sigma_{zz}(z)\ \sigma_{yz}(z)\ \sigma_{xz}(z)\right\}^{\mathrm{T}}, \tag{63}$$

$$\mathbf{s}_0(z) = \left\{\sigma_{xx}(z)\ \sigma_{yy}(z)\ \sigma_{xy}(z)\right\}^{\mathrm{T}}. \tag{64}$$

The dimensions of the matrices are $\left\{\mathbf{A}_i \in \mathbb{C}^{9\times9},\ i = \{a, b, x, y, z\}\right\}$.

$$\mathbf{A}_a\big|_i^j = \begin{cases} -1 & [i, j] = \{[1, 1], [2, 2], [3, 9], [4, 8], [5, 7], [6, 3]\} \\ 0 & \text{otherwise} \end{cases} \tag{65}$$

$$\mathbf{A}_b\big|_i^j, = \begin{cases} -\imath\omega\rho_s\mathbf{I}_3 & i = 7, \ldots, 9,\ j = 4, \ldots, 6, \\ 0 & \text{otherwise.} \end{cases} \tag{66}$$

$$\mathbf{A}_x\big|_i^j = \begin{cases} 1 & [i, j] = \{[7, 1], [8, 3], [9, 7]\} \\ \mathbf{C}^e\big|_{:}^{1} & i = 1, \ldots, 6,\ j = 4, \\ \mathbf{C}^e\big|_{:}^{6} & i = 1, \ldots, 6,\ j = 5, \\ \mathbf{C}^e\big|_{:}^{5} & i = 1, \ldots, 6,\ j = 6, \\ 0 & \text{otherwise.} \end{cases} \tag{67}$$

$$\mathbf{A}_y\big|_i^j = \begin{cases} 1 & [i,j] = \{[7,3],[8,2],[9,8]\} \\ \mathbf{C}^e\big|_{:}^{6} & i = 1,\ldots,6,\ \ j = 4, \\ \mathbf{C}^e\big|_{:}^{2} & i = 1,\ldots,6,\ \ j = 5, \\ \mathbf{C}^e\big|_{:}^{4} & i = 1,\ldots,6,\ \ j = 6, \\ 0 & \text{otherwise.} \end{cases} \tag{68}$$

$$\mathbf{A}_z\big|_i^j = \begin{cases} \mathbf{I}_3 & i = 7,\ldots,9,\ \ j = 7,\ldots,9, \\ \mathbf{C}^e\big|_{:}^{5} & i = 1,\ldots,6,\ \ j = 4, \\ \mathbf{C}^e\big|_{:}^{4} & i = 1,\ldots,6,\ \ j = 5, \\ \mathbf{C}^e\big|_{:}^{3} & i = 1,\ldots,6,\ \ j = 6, \\ 0 & \text{otherwise.} \end{cases} \tag{69}$$

A.3 Poroelastic media with light fluid/solid coupling under the Dazel $\{\mathbf{u}^s, \mathbf{u}^t\}$ representation

The dimensions of the matrices are $\left\{\mathbf{A}_i \in \mathbb{C}^{13\times 13},\ i = \{a,b,x,y,z\}\right\}$. The expression of the different coefficients may be found in the literature [1,18,30,32]. The formulation follows the notation in Parra Martinez *et al.* [43], where the correspondent state vector $\mathbf{s}(z)$ and redundant variables vector $\mathbf{s}_0(z)$ may be found.

$$\mathbf{A}_a\big|_i^j = \begin{cases} 1 & i = 7,\ \ j = 13, \\ -1 & [i,j] = \{[8,3],[9,4],[10,12],[11,11],[12,10],[13,5]\} \\ 0 & \text{otherwise} \end{cases} \tag{70}$$

$$\mathbf{A}_b\big|_i^j, = \begin{cases} -\imath\omega\tilde{\boldsymbol{\rho}}_s & i = 1,\ldots,3,\ \ j = 6,\ldots,8, \\ -\imath\omega\tilde{\boldsymbol{\rho}}_{eq}\tilde{\boldsymbol{\gamma}}_{eq} & i = 4,\ldots,6,\ \ j = 6,\ldots,8, \\ -\imath\omega\left[\tilde{\boldsymbol{\rho}}_{eq}\tilde{\boldsymbol{\gamma}}_{eq}\right]\big|_{:}^{1:2} & i = 1,\ldots,3,\ \ j = 1,\ldots,2, \\ -\imath\omega\left[\tilde{\boldsymbol{\rho}}_{eq}\tilde{\boldsymbol{\gamma}}_{eq}\right]\big|_{:}^{3} & i = 1,\ldots,3,\ \ j = 9, \\ -\imath\omega\tilde{\boldsymbol{\rho}}_{eq}\big|_{:}^{1:2} & i = 4,\ldots,6,\ \ j = 1,\ldots,2, \\ -\imath\omega\tilde{\boldsymbol{\rho}}_{eq}\big|_{:}^{3} & i = 4,\ldots,6,\ \ j = 9, \\ 0 & \text{otherwise.} \end{cases} \tag{71}$$

$$\mathbf{A}_x\big|_i^j = \begin{cases} 1 & [i,j] = \{[\,1,3],[2,5],[3,10]\} \\ -1 & i = 4,\ j = 13, \\ \tilde{K}_{eq} & i = 7,\ j = 1, \\ \hat{\mathbf{H}}\big|_:^1 & i = 8,\ldots,13,\ j = 6, \\ \hat{\mathbf{H}}\big|_:^6 & i = 8,\ldots,13,\ j = 7, \\ \hat{\mathbf{H}}\big|_:^5 & i = 8,\ldots,13,\ j = 8, \\ 0 & \text{otherwise.} \end{cases} \tag{72}$$

$$\mathbf{A}_y\big|_i^j = \begin{cases} 1 & [i,j] = \{[\,1,5],[2,4],[3,11]\} \\ -1 & i = 5,\ j = 13, \\ \tilde{K}_{eq} & i = 7,\ j = 2, \\ \hat{\mathbf{H}}\big|_:^6 & i = 8,\ldots,13,\ j = 6, \\ \hat{\mathbf{H}}\big|_:^2 & i = 8,\ldots,13,\ j = 7, \\ \hat{\mathbf{H}}\big|_:^4 & i = 8,\ldots,13,\ j = 8, \\ 0 & \text{otherwise.} \end{cases} \tag{73}$$

$$\mathbf{A}_z\big|_i^j = \begin{cases} \mathbf{I}_3 & i = 1,\ldots,3,\ j = 10,\ldots,12, \\ -1 & i = 6,\ j = 13, \\ \tilde{K}_{eq} & i = 7,\ j = 9, \\ \hat{\mathbf{H}}\big|_:^5 & i = 8,\ldots,13,\ j = 6, \\ \hat{\mathbf{H}}\big|_:^4 & i = 8,\ldots,13,\ j = 7, \\ \hat{\mathbf{H}}\big|_:^3 & i = 8,\ldots,13,\ j = 8, \\ 0 & \text{otherwise.} \end{cases} \tag{74}$$

A.4 Poroelastic media with heavy fluid/solid coupling under the Biot-Newton $\{\mathbf{u}^s, \mathbf{u}^f\}$ representation

The notations correspond to those in Carcione[11]. The state vector is detailed in Eq. (42). The dimensions of the matrices are $\left\{\mathbf{A}_i \in \mathbb{C}^{13\times 13},\ i = \{a,b,x,y,z\}\right\}$.

$$\mathbf{A}_a\big|_i^j = \begin{cases} -1 & [i,j] = \{[7,13],[8,3],[9,4],[10,12],[11,11],[12,10],[13,5]\} \\ 0 & \text{otherwise} \end{cases} \tag{75}$$

$$\mathbf{A}_b\big|_i^j, = \begin{cases} -\iota\omega\rho_f & i = 3,\ j = 9, \\ -\iota\omega\rho_f\,\mathbf{I}_2 & i = 1,\ldots,2,\ j = 1,\ldots,2, \\ -\iota\omega\rho\,\mathbf{I}_3 & i = 4,\ldots,6,\ j = 6,\ldots,8, \\ -\iota\omega\rho_s\,\mathbf{I}_3 & i = 1,\ldots,3,\ j = 6,\ldots,8, \\ -\iota\omega\mathbf{Y}\big|_:^{1:2} & i = 4,\ldots,6,\ j = 1,\ldots,2, \\ -\iota\omega\mathbf{Y}\big|_:^3 & i = 4,\ldots,6,\ j = 9, \\ 0 & \text{otherwise.} \end{cases} \tag{76}$$

$$\mathbf{A}_x\big|_i^j = \begin{cases} 1 & [i,j] = \{[1,3],[2,5],[3,10]\} \\ -1 & i = 4,\ j = 13, \\ M & i = 7,\ j = 1, \\ M\mathbf{a}\big|_1 & i = 7,\ j = 6, \\ M\mathbf{a}\big|_6 & i = 7,\ j = 7, \\ M\mathbf{a}\big|_5 & i = 7,\ j = 8, \\ M\mathbf{a} & i = 8,\ldots,13,\ j = 1, \\ \mathbf{C}\big|_:^1 & i = 8,\ldots,13,\ j = 6, \\ \mathbf{C}\big|_:^6 & i = 8,\ldots,13,\ j = 7, \\ \mathbf{C}\big|_:^5 & i = 8,\ldots,13,\ j = 8, \\ 0 & \text{otherwise.} \end{cases} \tag{77}$$

$$\mathbf{A}_y\big|_i^j = \begin{cases} 1 & [i,j] = \{[1,5],[2,4],[3,11]\} \\ -1 & i = 5,\ j = 13, \\ M & i = 7,\ j = 2, \\ M\mathbf{a}\big|_6 & i = 7,\ j = 6, \\ M\mathbf{a}\big|_2 & i = 7,\ j = 7, \\ M\mathbf{a}\big|_4 & i = 7,\ j = 8, \\ M\mathbf{a} & i = 8,\ldots,13,\ j = 2, \\ \mathbf{C}\big|_:^6 & i = 8,\ldots,13,\ j = 6, \\ \mathbf{C}\big|_:^2 & i = 8,\ldots,13,\ j = 7, \\ \mathbf{C}\big|_:^4 & i = 8,\ldots,13,\ j = 8, \\ 0 & \text{otherwise.} \end{cases} \tag{78}$$

$$\mathbf{A}_z\big|_i^j = \begin{cases} -1 & i = 6,\ j = 13, \\ M & i = 7,\ j = 9, \\ M\mathbf{a}\big|_5 & i = 7,\ j = 6, \\ M\mathbf{a}\big|_4 & i = 7,\ j = 7, \\ M\mathbf{a}\big|_3 & i = 7,\ j = 8, \\ M\mathbf{a} & i = 8,\ldots,13,\ j = 9, \\ \mathbf{C}\big|_:^5 & i = 8,\ldots,13,\ j = 6, \\ \mathbf{C}\big|_:^4 & i = 8,\ldots,13,\ j = 7, \\ \mathbf{C}\big|_:^3 & i = 8,\ldots,13,\ j = 8, \\ 0 & \text{otherwise.} \end{cases} \tag{79}$$

Bibliography

[1] Allard, J. F. and Atalla, N. (2009). *Propagation of Sound in Porous Media: Modelling Sound Absorbing Materials*. John Wiley & Sons, 2nd edition.

[2] Allard, J. F., Bourdier, R., and L'Esperance, A. (1987). Anisotropy effect in glass wool on normal impedance in oblique incidence. *Journal of Sound and Vibration*, 114(2):233–238.

[3] Allard, J. F., Dazel, O., Descheemaeker, J., Geebelen, N., Boeckx, L., and Lauriks, W. (2009). Rayleigh waves in air saturated axisymmetrical soft porous media. *Journal of Applied Physics*, 106(1).

[4] Biot, M. A. (1954). Theory of Stress-Strain Relations in Anisotropic Viscoelasticity and Relaxation Phenomena. *Journal of Applied Physics*, 25(11):1385–1391.

[5] Biot, M. A. (1955). Theory of elasticity and consolidation for a porous anisotropic solid. *Journal of Applied Physics*, 26(2):182–185.

[6] Biot, M. A. (1956a). Theory of deformation of a porous viscoelastic anisotropic solid. *Journal of Applied Physics*, 27(5):459–467.

[7] Biot, M. A. (1956b). Theory of Propagation of Elastic Waves in a Fluid-Saturated Porous Solid. I. Low-Frequency Range. *The Journal of the Acoustical Society of America*, 28(2):168–178.

[8] Biot, M. A. (1956c). Theory of Propagation of Elastic Waves in a Fluid-Saturated Porous Solid. II. Higher Frequency Range. *The Journal of the Acoustical Society of America*, 28(2):179–191.

[9] Biot, M. A. (1962). Generalized Theory of Acoustic Propagation in Porous Dissipative Media. *The Journal of the Acoustical Society of America*, 34(9A):1254.

[10] Cameron, C. J., Lind-Nordgren, E., Wennhage, P., and Göransson, P. (2014). On the balancing of structural and acoustic performance of a sandwich panel based on topology, property, and size optimization. *Journal of Sound and Vibration*, 333(13):2677–2698.

[11] Carcione, J. M. (2001). Energy Balance and Fundamental Relations in Dynamic Anisotropic Poro-Viscoelasticity. *Proceedings: Mathematical, Physical and Engineering Sciences*, 457(2006):331–348.

[12] Carcione, J. M. (2011). Electromagnetic diffusion in anisotropic media. *Radio Science*, 46(1):RS1010.

[13] Carcione, J. M. (2014). *Wave fields in real media: wave propagation in anisotropic, anelastic, porous and electromagnetic media*. Elsevier Science, 3 edition.

[14] Castagnède, B., Aknine, A., Melon, M., and Depollier, C. (1998). Ultrasonic characterization of the anisotropic behavior of air-saturated porous materials. *Ultrasonics*, 36(1-5):323–341.

[15] Cuenca, J. and Göransson, P. (2012). Inverse estimation of the elastic and anelastic properties of the porous frame of anisotropic open-cell foams. *The Journal of the Acoustical Society of America*, 132(2):621.

[16] Cuenca, J., Van der Kelen, C., and Göransson, P. (2014). A general methodology for inverse estimation of the elastic and anelastic properties of anisotropic open-cell porous materials—with application to a melamine foam. *Journal of Applied Physics*, 115(8):084904.

[17] D'Alessandro, V., Petrone, G., Franco, F., and De Rosa, S. (2013). A review of the vibroacoustics of sandwich panels: Models and experiments. *Journal of Sandwich Structures and Materials*, 15(5):541–582.

[18] Dazel, O., Brouard, B., Depollier, C., and Griffiths, S. (2007). An alternative Biot's displacement formulation for porous materials. *The Journal of the Acoustical Society of America*, 121(6):3509–3516.

[19] Dazel, O., Groby, J.-P., Brouard, B., and Potel, C. (2013). A stable method to model the acoustic response of multilayered structures. *Journal of Applied Physics*, 113(8):083506.

[20] Deckers, E., Atak, O., Coox, L., D'Amico, R., Devriendt, H., Jonckheere, S., Koo, K., Pluymers, B., Vandepitte, D., and Desmet, W. (2014). The wave based method: An overview of 15 years of research. *Wave Motion*, 51(4):550–565.

[21] Dovstam, K. (2000). Augmented Hooke's law based on alternative stress relaxation models. *Computational Mechanics*, 26(1):90–103.

[22] Fahy, F. and Gardonio, P. (2007). *Sound and Structural Vibration*. Burlington Academic Press, Burlington.

[23] Färm, A. (2016). *Absorption of Sound : On the effects of field interaction on absorber performance*. PhD thesis, KTH Royal Institute of Technology.

[24] Färm, A., Boij, S., Glav, R., and Dazel, O. (2016). Absorption of sound at a surface exposed to flow and temperature gradients. *Applied Acoustics*, 110:33–42.

[25] Göransson, P., Guastavino, R., and Hörlin, N.-E. (2009). Measurement and inverse estimation of 3D anisotropic flow resistivity for porous materials. *Journal of Sound and Vibration*, 327(3-5):354–367.

[26] Gorog, S., Panneton, R., and Atalla, N. (1997). Mixed displacement-pressure formulation for acoustic anisotropic open porous media. *Journal of Applied Physics*, 82(9):4192–4196.

[27] Groby, J.-P., Duclos, A., Dazel, O., Boeckx, L., and Lauriks, W. (2011). Absorption of a rigid frame porous layer with periodic circular inclusions backed by a periodic grating. *The Journal of the Acoustical Society of America*, 129(5):3035–3046.

[28] Guastavino, R. and Göransson, P. (2007). A 3D displacement measurement methodology for anisotropic porous cellular foam materials. *Polymer Testing*, 26(6):711–719.

[29] Gusikhin, O., Rychtyckyj, N., and Filev, D. (2007). Intelligent systems in the automotive industry: Applications and trends. *Knowledge and Information Systems*, 12(2):147–168.

[30] Hörlin, N.-E. and Göransson, P. (2010). Weak, anisotropic symmetric formulations of Biot's equations for vibro-acoustic modelling of porous elastic materials. *International Journal for Numerical Methods in Engineering*, 84(12):1519–1540.

[31] Jaouen, L., Renault, A., and Deverge, M. (2008). Elastic and damping characterizations of acoustical porous materials: Available experimental methods and applications to a melamine foam. *Applied Acoustics*, 69(12):1129–1140.

[32] Khurana, P., Boeckx, L., Lauriks, W., Leclaire, P., Dazel, O., and Allard, J. F. (2009). A description of transversely isotropic sound absorbing porous materials by transfer matrices. *The Journal of the Acoustical Society of America*, 125(May 2011):915–921.

[33] Lewis, R. and Schrefler, B. (1998). *Finite Element Method in the Deformation and Consolidation of Porous Media*. John Wiley and Sons Inc.,New York, NY.

[34] Lind-Nordgren, E., Göransson, P., Deü, J.-F., and Dazel, O. (2013). Vibroacoustic response sensitivity due to relative alignment of two anisotropic poro-elastic layers. *The Journal of the Acoustical Society of America*, 133(5):EL426–30.

[35] Lundberg, O. E., Finnveden, S., Björklund, S., Pärssinen, M., and Lopez Arteaga, I. (2015). A nonlinear state-dependent model for vibrations excited by roughness in rolling contacts. *Journal of Sound and Vibration*, 345:197–213.

[36] Melon, M. (1998). Acoustical and mechanical characterization of anisotropic open-cell foams. *The Journal of the Acoustical Society of America*, 104(5):2622–2627.

[37] Melon, M., Lafarge, D., Castagnède, B., and Brown, N. (1995). Measurement of tortuosity of anisotropic acoustic materials. *Journal of Applied Physics*, 78(8):4929–4932.

[38] Miettinen, K. (1998). *Nonlinear Multiobjective Optimization*, volume 12 of *International Series in Operations Research & Management Science*. Springer US, 1 edition.

[39] Mrazova, M. (2013). Advanced composite materials of the future in aerospace industry. *INCAS BULLETIN*, 5(3):139–150.

[40] Norris, A. N. (2006). The isotropic material closest to a given anisotropic material. *Journal of Mechanichs of Materials and Structures*, 1(2):223–238.

[41] Österlöf, R., Wentzel, H., and Kari, L. (2015). An efficient method for obtaining the hyperelastic properties of filled elastomers in finite strain applications. *Polymer Testing*, 41:44–54.

[42] Parra Martinez, J. P. (2015). *On the ECO2 multifunctional design paradigm and tools for acoustic tailoring*. PhD thesis, KTH Royal Institute of Technology, Stockholm.

[43] Parra Martinez, J. P., Dazel, O., Göransson, P., and Cuenca, J. (2016a). Acoustic analysis of anisotropic poroelastic multilayered systems. *Journal of Applied Physics*, 119(8):084907.

[44] Parra Martinez, J. P., Dazel, O., Göransson, P., and Cuenca, J. (2016b). Derivation of the state matrix for dynamic analysis of linear homogeneous media. *The Journal of the Acoustical Society of America*, 140(2):EL218–EL220.

[45] Parra Martinez, J. P., Göransson, P., Dazel, O., and Cuenca, J. (2014). Analysis of the frequency response behaviour of anisotropic multilayered structures and potential acoustic performance optimizations. In *ISMA-USD*, pages 4375–4386.

[46] Parra Martinez, J. P., Göransson, P., Dazel, O., Cuenca, J., and Jaouen, L. (2016c). Wave analysis of intrinsic phenomena related to anisotropic poroelastic materials in multilayered systems. In *ISMA-USD*, pages 513–520.

[47] Perrot, C., Chevillotte, F., Tan Hoang, M., Bonnet, G., Bécot, F.-X., Gautron, L., and Duval, A. (2012). Microstructure, transport, and acoustic properties of open-cell foam samples: Experiments and three-dimensional numerical simulations. *Journal of Applied Physics*, 111(1):014911.

[48] Pride, S. R. and Berryman, J. G. (1998). Connecting theory to experiment in poroelasticity. *Journal of the Mechanics and Physics of Solids*, 46(4):719–747.

[49] Pride, S. R. and Garambois, S. (2002). The role of Biot slow waves in electroseismic wave phenomena. *The Journal of the Acoustical Society of America*, 111(2):697–706.

[50] Pritz, T. (1996). Analysis of four-parameter fractional derivative model of real solid materials. *Journal of Sound and Vibration*, 195(1):103–115.

[51] Rice, H. and Göransson, P. (1999). A dynamical model of light fibrous materials. *International Journal of Mechanical Sciences*, 41(4-5):561–579.

[52] Rynell, A., Efraimsson, G., Chevalier, M., and Abom, M. (2016). Acoustic characteristics of a heavy duty vehicle cooling module. *Applied Acoustics*, 111:67–76.

[53] Serra, Q., Ichchou, M. N., and Deü, J.-F. (2015). On the Use of Transfer Approaches to Predict the Vibroacoustic Response of Poroelastic Media. *Journal of Computational*

Acoustics, 23:1550020.

[54] Sharma, M. (2004). Three-dimensional wave propagation in a general anisotropic poroelastic medium: Phase velocity, group velocity and polarization. *Geophysical Journal International*, 156(2):329–344.

[55] Shaw, A., Dayyani, I., and Friswell, M. (2015). Optimisation of composite corrugated skins for buckling in morphing aircraft. *Composite Structures*, 119:227–237.

[56] Slawinski, M. A. (2010). *Waves and Rays in Elastic Continua*. World Scientific.

[57] Svanberg, K. (1987). The method of moving asymptotes—a new method for structural optimization. *International Journal for Numerical Methods in Engineering*, 24(2):359–373.

[58] Svanberg, K. (2006). A Class of Globally Convergent Optimization Methods Based on Conservative Convex Separable Approximations. *SIAM Journal on Optimization*, 12(2):555–573.

[59] Thompson, M. and Willis, J. R. (1991). A Reformation of the Equations of Anisotropic Poroelasticity. *Journal of Applied Mechanics*, 58(3):612–616.

[60] Van der Kelen, C., Cuenca, J., and Göransson, P. (2015a). A method for characterisation of the static elastic properties of the porous frame of orthotropic open-cell foams. *International Journal of Engineering Science*, 86(0):44–59.

[61] Van der Kelen, C., Cuenca, J., and Göransson, P. (2015b). Property modelling A method for the inverse estimation of the static elastic compressional moduli of anisotropic poroelastic foams e With application to a melamine foam. *Polymer Testing*, 43:123–130.

[62] Van der Kelen, C. and Göransson, P. (2013). Identification of the full anisotropic flow resistivity tensor for multiple glass wool and melamine foam samples. *The Journal of the Acoustical Society of America*, 134(6):4659.

[63] Van der Kelen, C., Göransson, P., Pluymers, B., and Desmet, W. (2014). On the influence of frequency-dependent elastic properties in vibro-acoustic modelling of porous materials under structural excitation. *Journal of Sound and Vibration*, 333(24).

[64] Wang, Z. and Norris, A. N. (1995). Waves in cylindrical shells with circumferential submembers: a matrix approach. *Journal of Sound and Vibration*, 181(3):457–484.

[65] Wennberg, D. (2013). *Multi-Functional Composite Design Concepts for Rail Vehicle Car Bodies*. PhD thesis, KTH, The KTH Railway Group, Stockholm, Sweden.

[66] Wennberg, D. and Stichel, S. (2014). Multi-functional Design of a Composite High-Speed Train Body Structure. *Structural and Multidisciplinary Optimization*, 50(3):475–488.

Part 2

Appended publications